

Water Resources Research

RESEARCH ARTICLE

10.1029/2018WR023703

Key Points:

- Slow (epikarst and phreatic) flows account for nearly 90% of nitrate loading in an agricultural-karst system
- Nitrate accumulation and subsequent leaching dominate pathway processes
- Agricultural-karst systems act as detention basins of nitrate and, during flood recession, drain storm-derived nitrate more gradually compared to poorly karstified systems

Supporting Information:

- Supporting Information S1

Correspondence to:

A. Husic,
ahusic@ku.edu

Citation:

Husic, A., Fox, J., Adams, E., Ford, W., Agouridis, C., Currens, J., & Backus, J. (2019). Nitrate pathways, processes, and timing in an agricultural karst system: Development and application of a numerical model. *Water Resources Research*, 55, 2079–2103. <https://doi.org/10.1029/2018WR023703>





Received 20 JUL 2018

Accepted 18 FEB 2019

Accepted article online 25 FEB 2019

Published online 14 MAR 2019

Nitrate Pathways, Processes, and Timing in an Agricultural Karst System: Development and Application of a Numerical Model

A. Husic¹ , J. Fox² , E. Adams² , W. Ford³, C. Agouridis³, J. Currens⁴, and J. Backus⁴ 

¹Department of Civil, Environmental, and Architectural Engineering, University of Kansas, Lawrence, Kansas, USA, ²Department of Civil Engineering, University of Kentucky, Lexington, Kentucky, USA, ³Department of Biosystems and Agricultural Engineering, University of Kentucky, Lexington, Kentucky, USA, ⁴Kentucky Geological Survey, Lexington, Kentucky, USA

Abstract Nitrogen (N) contamination within agricultural-karst landscapes and aquifers is widely reported; however, the complex hydrological pathways of karst make N fate difficult to ascertain. We developed a hydrologic and N numerical model for agricultural-karst, including simulation of soil, epikarst, phreatic, and quick flow pathways as well as biochemical processes such as nitrification, mineralization, and denitrification. We tested the model on four years of nitrate (NO_3^-) data collected from a phreatic conduit and an overlying surface channel in the Cane Run watershed, Kentucky, USA. Model results indicate that slow to moderate flow pathways (phreatic and epikarst) dominate the N load and account for nearly 90% of downstream NO_3^- delivery. Further, quick flow pathways dilute NO_3^- concentrations relative to background aquifer levels. Net denitrification distributed across soil, epikarst, and phreatic water removes approximately 36% of the N inputs to the system at rates comparable to nonkarst systems. Evidence is provided by numerical modeling that NO_3^- accumulation via evapotranspiration in the soil followed by leaching through the epikarst acts as a control on spring NO_3^- concentration and loading. Compared to a fluvial-dominated immature karst system, mature-karst systems behave as natural detention basins for NO_3^- , temporarily delaying NO_3^- delivery to downstream waters and maintaining elevated NO_3^- concentrations for days to weeks after hydrologic activity ends. This study shows the efficacy of numerical modeling to elucidate complex pathways, processes, and timing of N in karst systems.

1. Introduction

Nitrogen (N) contamination within agricultural-karst landscapes and aquifers is widely reported; however, the complex hydrological pathways of karst make N fate difficult to estimate. In nonkarst agricultural landscapes, pathways of N transport to streams are dilute quick flow, concentrated quick flow, and slow flow groundwater (Miller et al., 2017; Tesoriero et al., 2013). Karst agricultural systems receive similar N inputs as nonkarst agriculture because karst topography is often gently rolling making it suitable for livestock production and row cropping (Boyer & Pasquarell, 1995). N pathways are more complex in karst systems as a result of a quick flow groundwater component associated with sinking streams, epikarst fracture networks, and subsurface caves and conduits (Pronk et al., 2009; White, 2002). The quick flow component to karst groundwater obscures our understanding of N fate in these karst systems. Three current research gaps for karst hydrology include our knowledge of (i) dominant karst pathways controlling N fate in different systems, (ii) the relative importance of physical versus biogeochemical processes to control N fate in karst, and (iii) the timing of N delivered to karst springs from different sources (Jones & Smart, 2005; Opsahl et al., 2017; Yue et al., 2015). Our motivation was to provide knowledge for filling these research gaps for karst by advancing and applying numerical modeling that can identify dominant N pathways, processes, and timing in agricultural-karst systems.

With respect to the dominant pathways controlling N fate, we question the relative importance of quick flow versus slow flow pathways for controlling N fluxes. N pathway emphasis has been placed on aquifer contamination via quick flow pathways due in part to the optical nature of entire streams sinking into the subsurface (Mahler & Garner, 2009). However, we hypothesize that slow flow is the dominant N pathway in agricultural-karst. Two ideas from our review of current literature bring us to this hypothesis. First, we

Table 1

Review Table of NO_3^- Studies Conducted in Karst Watersheds ($n = 22$) Showing Study Location, the Concentration of Quick Flow NO_3^- , and the Concentration of Discharged Aquifer NO_3^-

Study Site/Reference	Location	Quick Flow NO_3^- (mg N/L) ^a	Aquifer NO_3^- (mg N/L) ^b
Royal Spring (<i>present study</i>)	Kentucky, USA	1.92	2.86
Barton Springs (Mahler and Garner, 2009)	Texas, USA	0.05	0.34
Los Tajos (Mudarra et al., 2014)	Malaga, Spain	0.43	2.53
Barton Springs (Mahler et al., 2008)	Texas, USA	0.29	1.56
San Antonio Edwards Aquifer (Musgrove et al., 2016)	Texas, USA	0.43	1.86
Fountain Creek Watershed (Stueber and Criss, 2005)	Illinois, USA	2.80	4.20
Wakulla Springs (Katz et al., 2004)	Florida, USA	0.02	0.80
Guiyang Basin (Liu et al., 2006)	Guizhou, China	2.14	4.15
Stafford Springs (Davis et al., 1995; Peterson et al., 2002)	Arkansas, USA	1.50	5.10
Umm Rijam Aquifer (Obeidat et al., 2008)	Yarmouk, Jordan	0.61	7.45
Yverdon-les-Bains System (Pronk et al., 2009)	Jura, Switzerland	6.75	1.96
Big Spring Basin (Rowden et al., 1998, 2001)	Iowa, USA	7.61	9.93
Jiangjia Spring (He et al., 2010)	Chongqing, China	0.79	5.01
Spring Creek Watershed (Buda and DeWalle, 2009)	Pennsylvania, USA	2.80	4.47
Springbrook Creek Watershed (Schilling and Helmers, 2008)	Iowa, USA	0.10	12.08
Pays de Caux System (Fournier et al., 2007)	Norville, France	2.40	4.86
Houzhai Catchment (Yue et al., 2015)	Guizhou, China	2.58	3.62
Vransko Polje (Markovic et al., 2006)	Zagreb, Croatia	0.20	2.13
Kestel Polje-Kirkgoz Springs (Ekmekci, 2005)	Antalya, Turkey	1.20	0.70
Plainview System (Mooers and Alexander, 1994)	Minnesota, USA	16.85	12.90
Jackson and Cleghorn Springs (Swanson, 2004; Long et al., 2008)	South Dakota, USA	0.10	0.31
Funshion River Watershed (Fenton et al., 2017)	Fermoy, Ireland	12.04	11.80

Note. Eighteen of 22 (82%) studies reported higher NO_3^- concentrations in aquifer water than in quick flow water.

^aMean value shown is that of the surface stream(s) or other reported quick flow sources (e.g., rain). ^bMean value shown is that of the spring(s) (if available) or other aquifer values (e.g., wells).

analyzed data from 22 karst studies (Table 1) reporting N data for quick flow and slow flow NO_3^- pathways. We found that 18 out of 22 (82%) of the studies show higher NO_3^- concentrations for slow flow as compared to quick flow. Second, recent water budget studies in karst discuss large water storage volumes within the epikarst and phreatic reservoirs and their potential to dominate water exports even in karst systems with high surface connectivity (Aquilina et al., 2006; Knierim et al., 2013; Toran & White, 2005; Williams, 2008). High NO_3^- concentrations in slow flow water and large storage volumes within slow flow reservoirs suggest the potential for their dominant control on net N export from karst aquifers.

With respect to dominant process, we question the relative importance of physical versus biogeochemical processes to control N fate in karst. Karst research suggests the potential for physical building-up and then leaching of soil nitrate as controlling N transport in agricultural-karst (Baran et al., 2008), with one study reporting increased nitrate concentration with percent of agricultural cover (Boyer & Alloush, 2001). However, the longer residence time of slow flow pathways suggest the potential for biogeochemical transformations to augment N contamination (Albertin et al., 2012; Han et al., 2015). Untangling the relative importance of physical and biogeochemical processes in karst using only field data is complicated by the extremely heterogenous geologic properties of calcium carbonate rock.

With respect to the timing of N delivery to karst springs from different sources, we question the time distribution of N export from side-by-side comparisons of a karst-dominated watershed with an adjacent fluvial-dominated immature karst watershed. Such a comparison allows for an understanding of how quick flow groundwater may be superimposed onto a hydrograph along with other surface water and groundwater sources. Side-by-side comparison of karst and nonkarst terrains provides valuable insight because terrain with karst potential experiences competition between fluvial and karst development (Ghasemzadeh et al., 2012). Further, karst landscape in some regions can be organized into discrete zones dominated by either karst- or fluvial-dominated features to the near-exclusion of the other (Phillips et al., 2004). Therefore,

such side-by-site geomorphologic organization allows us to study N timing in karst as compared to its fluvial counterpart and gain insight regarding the N timing of quick flow groundwater.

Knowledge for filling research gaps of karst pathways, processes, and timing may be gained by advancing and applying numerical models. Numerical model development for N in karst is needed because existing tools have several limitations. Off-the-shelf watershed water quality models (e.g., SWAT, HSPF) have been applied to karst nutrient studies with some success (Nikolaidis et al., 2013; Palanisamy & Workman, 2014); however, the models tend to be extrapolated beyond their hydrologic structure given the turbulent flow of the karst subsurface requiring empirical augmentation to allow adequate model calibration (Palanisamy & Workman, 2014). Graphical methods to apportion N loads to fast, intermediate, and slow flow pathways are robust (Fenton et al., 2017; Husic et al., 2019; Mellander et al., 2012), but limited in that they do not explicitly quantify internal N fate nor do they provide forecasting ability. Other karst-specific nutrient models assume that N is conservative (Mahler & Garner, 2009; Mudarra et al., 2014); however, we know that N transformation occurs in karst (Cohen et al., 2007; Henson et al., 2017; Katz et al., 2010; Panno et al., 2001).

We argue the reservoir modeling approach provides a suitable choice for N pathway, process, and timing estimates in karst. Reservoir-based models are increasingly used to estimate water transport in karst given their ability to accurately reflect multiple pathways (e.g., Fleury et al., 2007; Hartmann et al., 2014; Tritz et al., 2011). The reservoir approach shown by Fleury et al. and others for karst water transport has not yet been widely applied to the N fate problem (a relatively recent example is Hartmann et al. (2016)), yet the approach is suitable because of advantages associated with (i) simulating nonconservative N in the subsurface, (ii) representing many subsurface pathways as well as surface overflows, (iii) ease of coupling with long-term multiyear data streams, and (iv) including robust uncertainty routines coupled to high-performance computing. While the reservoir approach is attractive, issues with model suitability and equifinality (defined as the existence of multiple “acceptable” representations of an environmental system; Beven, 2006) must be addressed through rigorous evaluation of the model’s process-representation capability (Hartmann et al., 2013, 2017; Hartmann, 2017). Additionally, equifinality and uncertainty can be reduced through coupling multiple data streams (e.g., Ford et al., 2017). Therefore, in this paper, we develop a robust reservoir modeling approach for karst water and N capable of representing field processes and data streams.

Our objectives were to (1) collect four years of N data, identify the appropriate numerical model structure, develop a reservoir-based numerical model for N fate and transport, and apply it to an agricultural-karst system and (2) investigate the pathways controlling N transport, the net effect of physical and biogeochemical processes on N export, and the timing of N exports from a mature karst relative to an immature, fluvial-dominated counterpart. These two objectives provide the structural subheadings for sections 2 and 3 of the paper.

2. Methods

2.1. Numerical Model Development and Application

2.1.1. Theoretical Basis for Model

The theoretical background provides the context behind our conceptual model of pathways and processes impacting N in agricultural-karst (Figure 1). Surface to subsurface pathways can most broadly be separated into concentrated or diffuse N recharge (White, 2002). This broad division is further subdivided considering the three porosities that influence N recharge in karst: primary (matrix), secondary (fracture), and tertiary (conduit; White, 2002). Quick flow pathways convey concentrated N recharge through tertiary porosity voids such as sinkholes, swallets, and estavelles. As is typical of many karst systems, surface streams are event-activated and run dry for large parts of the year as a result of flow pirating by quick flow pathway karst features (Husic, Fox, Agouridis, et al., 2017). Diffuse recharge follows soil, epikarst, and phreatic zone pathways where storage volumes are several orders of magnitude greater than that of the quick flow pathways and have the potential to retain N (Bottrel & Atkinson, 1992; Williams, 2008). Dynamic soil and epikarst storages provide the potential for N accumulation and leaching processes to act as important mechanisms affecting net NO_3^- exports (Aquilina et al., 2006; Husic et al., 2019; Tzoraki & Nikolaidis, 2007). Phreatic pathways are sustained by Darcian groundwater recharge from stored volumes in the aquifer bedrock and are characterized by long residence times of water and N (Ghasemzadeh et al., 2012). Our concept (Figure 1) is

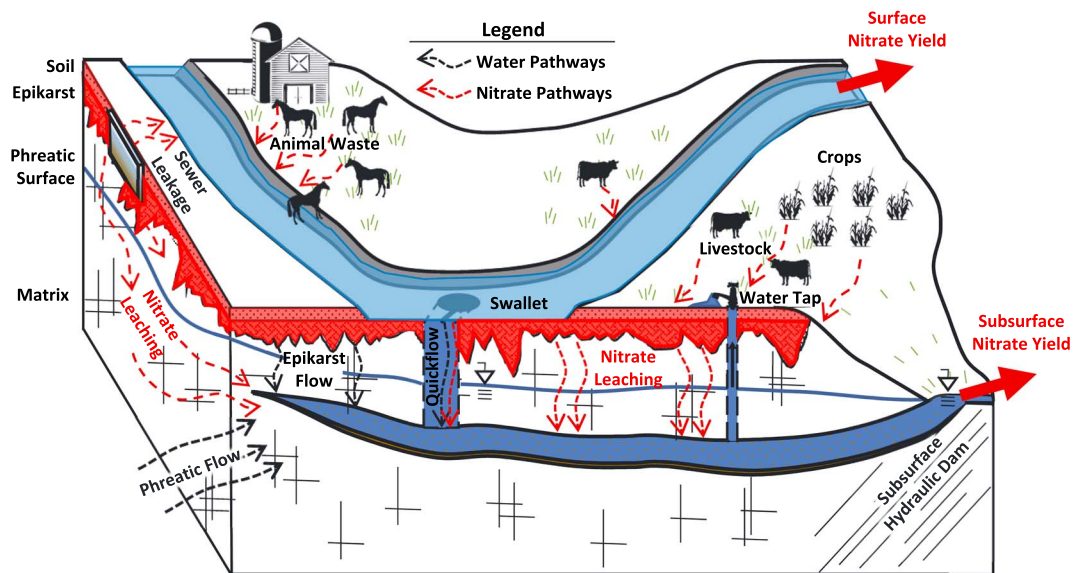


Figure 1. Conceptual model of water and NO_3^- pathways in an agricultural karst system. Contaminant provenance includes surface, subsurface, distributed, and point sources and pathways. The accumulation of NO_3^- within the karst aquifer followed by a release to the primary conduit results in NO_3^- leaching losses to downstream waterbodies.

consistent with numerous studies focused on water movement and N recharge in karst (e.g., Hartmann et al., 2016; Tritz et al., 2011).

We investigate N pathways, processes, and timing with the described conceptual model in mind. We designed a study to sample N from a sinking stream and subsurface conduit, and we use a numerical reservoir model to simulate pathways that cannot be measured directly in the field. We formulated the model using a system of cascading linear reservoirs to represent storage and conveyance zones (i.e., soil, epikarst, phreatic/matrix, and quick flow). This model structure was compared to, and outperformed, simpler one, two, and three reservoir model structures (Figure S1). The model simulates solute (nitrate, ammonium, and dissolved organic nitrogen) fate from recharge source to eventual downstream loading to the spring as well as the surface stream. We do not consider chemoautotrophic pathways as the study watershed is relatively rich in the energetically favorable organic carbon electron donor (Husic, Fox, Agouridis, et al., 2017; Husic, Fox, Ford, et al., 2017). Our study assumes temperate agricultural surface processes, mature karst subsurface development, coupled surface-subsurface pathways, and daily mixing of solutes after accounting for mass changes.

2.1.2. Study Site for Model Application

The Royal Spring groundwater basin (58 km^2) drains part of the Cane Run watershed (96 km^2) located in the Inner Bluegrass Region of Kentucky, USA (Figure 2). The land surface is primarily agricultural in use (60%) with highly urbanized headwaters (40%) and a temperate climate (mean annual temperature: $13.0 \pm 0.7 \text{ }^\circ\text{C}$, mean annual precipitation: $1,170 \pm 200 \text{ mm}$). The land surface is composed of moderately deep, well-drained soils underlain by phosphatic limestone of the Middle Ordovician period. Epikarst features are visible throughout the watershed both in naturally exposed karren as well as roadcuts. More than 50 swallets, estavelles, and sinks have been identified within Cane Run creek. The creek runs dry for approximately 90% of the year due to flow pirating by the subsurface drainage (Husic, Fox, Agouridis, et al., 2017). Epikarst pathways are likely the cause for peak storm-mobilized nutrient concentrations in the watershed (Husic et al., 2019). Anastomosing subsurface conduits converge to a primary phreatic cavern, 20 m below the ground surface, closely aligned with the overlying creek. The phreatic conduit supplies the primary basin outlet, Royal Spring (243 m above sea level), with an average perennial discharge of $0.67 \text{ m}^3/\text{s}$. The Royal Spring aquifer supplies water for distilleries, grist mills, horse farms, and crop irrigation, and the main springhead serves as the raw municipal water source for the City of Georgetown, Kentucky. The urbanization of the uplands has resulted in bacteria and nutrient loadings that exceed standards set by the Clean Water Act and Kentucky Division of Water (University of Kentucky College of Agriculture Food and the

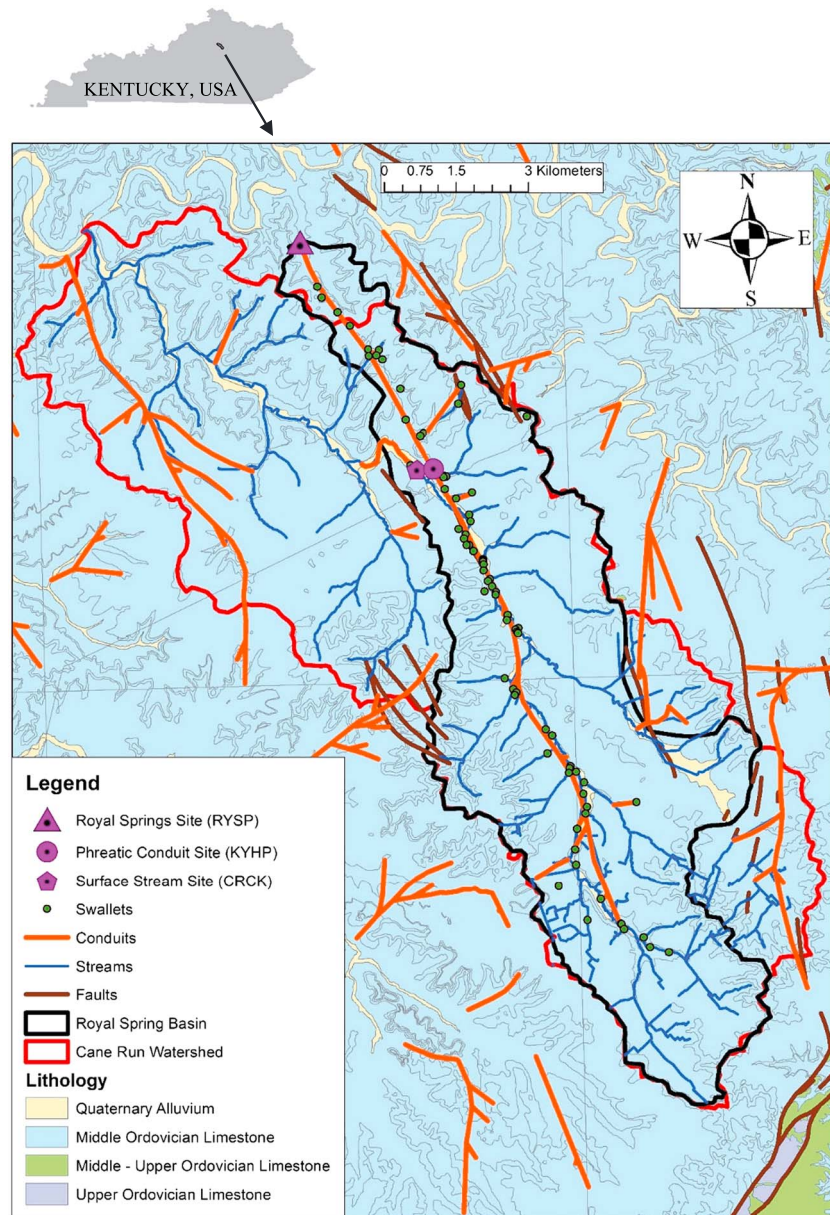


Figure 2. Cane Run watershed and Royal Spring Basin, including important sampling locations, swallets, conduits, streams, faults, drainage delineations, and lithology. Flow direction in surface streams and subsurface conduits is primarily from southeast to the northwest.

Environment (UKCAFE), 2011). The high surface-subsurface flow path connectivity has been suggested as the primary cause for the deterioration of water quality at the spring (UKCAFE, 2011). The watershed has been a karst research site led by the Kentucky Geological Survey and the University of Kentucky the past 40 years (Husic, Fox, Agouridis, et al., 2017; Husic, Fox, Ford, et al., 2017; Husic et al., 2019; Paylor & Currens, 2004; Spangler, 1982; Taylor, 1992; Thrailkill et al., 1991; Zhu et al., 2011).

Meteorological data were available from the Bluegrass Airport (NOAA ID USW00093820) as well as three nearby rain gauges (NOAA IDs US1KYSC0001, US1KYFY0009, and USC00153194). The gauge stations recorded relative humidity, temperature, solar radiation, and wind speed. Soil temperature was recorded at Spindletop Research Farm near the center of the basin (University of Kentucky Agriculture Weather Center (UKAg), 2007). There are three primary water sampling stations in the basin, including the primary spring (RYS), the longitudinal midpoint of the main phreatic conduit (KYHP), and a surface overflow

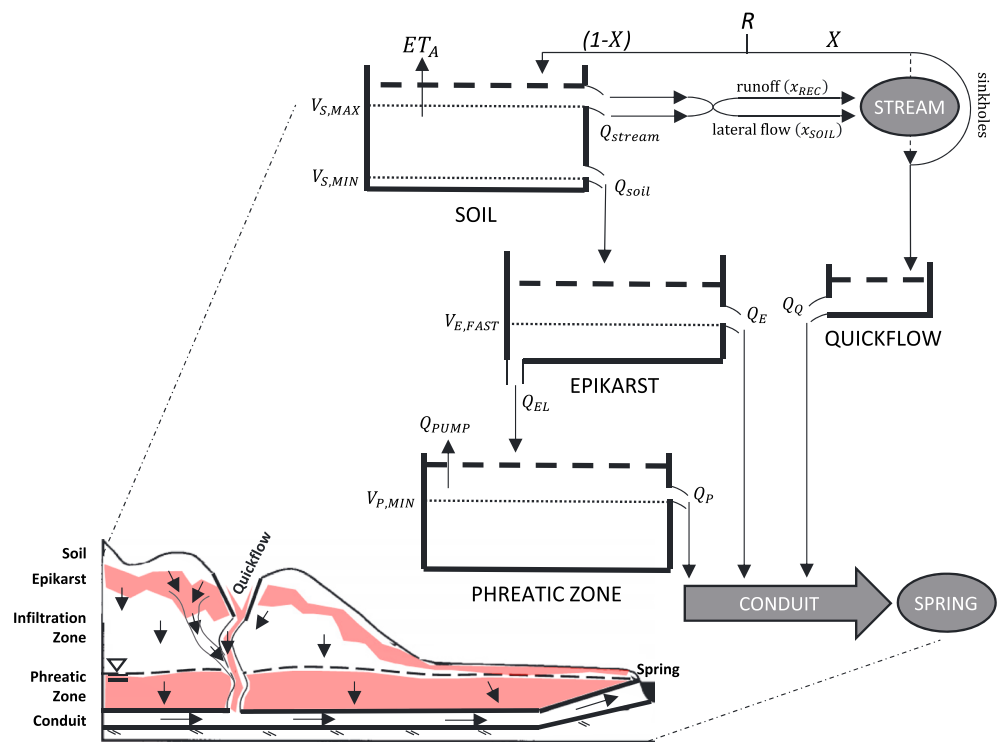


Figure 3. Model framework for water and nitrogen processes and pathways in a karst aquifer. Recharge (R) of water, NO_3^- , NH_4^+ , and DON is applied as concentrated input to the quick flow reservoir (X) or as distributed input to soil ($1 - X$). Distributed recharge of NO_3^- , NH_4^+ , and DON represents bulk infiltration of material (e.g., precipitation, fertilizer, manure, and sewage) to the soil. Evapotranspiration (ET_A), flow to surface stream (Q_{stream}) which includes runoff (x_{REC}) and lateral soil flow (x_{SOIL}) fractions, and percolation (Q_{soil}) are outflows from the soil reservoir. Soil field capacity is represented by $V_{S,MIN}$ and saturation conditions by $V_{S,MAX}$. Concentrated recharge to the quick flow reservoir includes sinkholes, swallets, and stream abstractions (dashed line). Outflow from the quick flow reservoir (Q_Q) occurs via shaft, sinkhole, and swallet discharge to the conduit. The epikarst is recharged by soil percolation and discharges water via seepage to the phreatic aquifer (Q_{EL}) or as conduit recharge via larger fractures (Q_E). Direct flow from the epikarst to the conduit occurs when dynamic storage within the epikarst exceeds a threshold ($V_{E,FAST}$). Finally, the phreatic zone is recharged by the epikarst and losses are attributed to diffuse flow (Q_P) and pumping losses (Q_{PUMP}) related to agricultural and other human demands. The level at which baseflow to the spring ceases (i.e., the spring runs dry) is represented by $V_{P,MIN}$.

stream (CRCK). The spring is operated by the United States Geological Survey (03288110). The Cane Run creek surface water overflow site is only active during high rainfall storm events. The longitudinal midpoint of the primary phreatic conduit is observed by a series of groundwater wells that directly intersect it (Husic, Fox, Agouridis, et al., 2017; Zhu et al., 2011). Water data collection and analyses for the study site were previously published in Husic, Fox, Agouridis, et al. (2017) and Husic, Fox, Ford, et al. (2017). Weekly maximum flows at the Phreatic Conduit (PC) and Royal Spring (RS) sites are similar in magnitude ($Q_{RS} = 0.99 \times Q_{PC}$, $R^2 = 0.77$; Husic, 2015); thus, we assume few water inputs/outputs along this section. Likewise, NO_3^- sampling at the two sites showed a nearly 1:1 relationship in NO_3^- concentration ($\text{NO}_3^-_{RS} = 1.06 \times \text{NO}_3^-_{PC}$, $R^2 = 0.81$; Kentucky Geological Survey, unpublished data), allowing us to use data from RYSP or KYHP to assist with numerical model calibration.

2.1.3. Numerical Model Formulation

We tested six possible model structures for representing water and N in karst, ranging from one to four reservoirs and from global to reservoir-specific N parameterization (see Figure S1). The formulation described herein is for the eventual “best fit” model structure, the four-reservoir model with global nitrogen parameterization. The results of the model structure evaluation are described later in section 3.

Numerical model formulation begins with the quick flow and soil reservoirs receiving concentrated and distributed recharge, respectively, which initializes the hierarchal model structure (Figure 3).

Precipitation input was estimated using the Thiessen polygon method, which calculates an area-weighted average of precipitation given multiple rain gauges (Goovaerts, 2000). Of this area-weighted average, the quick flow reservoir receives an X fraction to represent concentrated recharge via swallets, sinkholes, and stream abstractions. The soil reservoir receives the remaining $1 - X$ fraction as distributed recharge. A constant separation factor was chosen as most quick flow events in the watershed occur within the model time step (i.e., one day). Due to their proximity to the surface and relative shallowness compared to the rest of the aquifer, several earlier models combine the soil and epikarst storages into a single lumped reservoir (e.g., Tritz et al., 2011), but the two have been separated in this work to highlight evapotranspiration and lateral flow processes that primarily occur within the soil and dynamic storage that occurs in the epikarst (Aquilina et al., 2006; Williams, 2008). Potential evapotranspiration (ET_P) was modeled using the Penman-Montieth method which considers a reference crop type (i.e., grass, as much of the watershed consists of pasture). Actual evapotranspiration (ET_A) was modeled as a function of soil water content and ET_P (mm/day) as

$$ET_{A(i)} = \min[ET_{P(i)}, ET_{P(i)} \times (V_{S(i)}/V_{S,MAX})] \Delta t, \quad (1)$$

where $V_{S(i)}$ is the volume of water in the soil reservoir at time step i (mm), $V_{S,MAX}$ is the soil saturation depth (mm), and Δt is the model time step (day). This linear formulation of ET_A is consistent with reservoir model applications in other karst environments (e.g., Chang et al., 2017; Hartmann, 2017).

The mass balance of water within the soil reservoir (V_S) was discretized as

$$V_{S(i)} = V_{S(i-1)} + (R_{(i)}(1-X) - ET_{A(i)} - Q_{stream(i)} - Q_{soil(i)}) \Delta t, \quad (2)$$

where $V_{S(i-1)}$ is the volume of water in the soil reservoir at the end of the previous time step (mm), $R_{(i)}$ is the recharge from precipitation input (mm/day), $1 - X$ is the fraction of total recharge that infiltrates the soil reservoir, $Q_{stream(i)}$ is the lateral flow into the surface stream occurring only after soil saturation (mm/day), and $Q_{soil(i)}$ is the soil percolation to the epikarst (mm/day).

The model utilizes the linear discharge law, which relates discharge (Q) as the product of available head ($V - V_{MIN}$) and a discharge coefficient (α or k). As an example, soil discharge to the surface stream (Q_{stream}) was calculated as

$$Q_{stream(i)} = \max[0, k_{stream}(V_{S(i-1)} - V_{S,MAX}) \Delta t], \quad (3)$$

where k_{stream} is the discharge coefficient for runoff and lateral flow to the surface stream (day^{-1}). Analogous relationships were used for the remaining discharges (coefficients) in Figure 3: soil percolation (Q_{soil} , k_{soil}), slow epikarst percolation (Q_{EL} , k_{EL}), fast epikarst discharge (Q_E , α_2), concentrated quick flow (Q_Q , α_1), and phreatic slow flow (Q_P , α_3).

The mass balance of water within the epikarst reservoir (V_E) was modeled as

$$V_{E(i)} = V_{E(i-1)} + (Q_{soil(i)} - Q_{E(i)} - Q_{EL(i)}) \Delta t, \quad (4)$$

where $V_{E(i-1)}$ is the volume of water in the epikarst reservoir at the end of the previous time step (mm), $Q_{E(i)}$ is the fast component of epikarst discharge (mm/day) arising from preferential flow in large fractures that are well connected to the conduit, and $Q_{EL(i)}$ is the slower percolation of water through the vadose zone to the phreatic zone (mm/day).

The mass balance of water within the phreatic reservoir (V_P) was represented as

$$V_{P(i)} = V_{P(i-1)} + (Q_{EL(i)} - Q_{PUMP(i)} - Q_{P(i)}) \Delta t, \quad (5)$$

where $V_{P(i-1)}$ is the volume of water in the phreatic reservoir at the end of the previous time step (mm), $Q_{PUMP(i)}$ is the pumping rate from the aquifer (mm/day), and $Q_{P(i)}$ is the phreatic baseflow to the conduit (mm/day).

The balance of water within the quick flow reservoir (V_Q) has a single input from concentrated recharge and was formulated as

$$V_{Q(i)} = V_{Q(i-1)} + (R_{(i)} \cdot X - Q_{Q(i)}) \Delta t, \quad (6)$$

where $V_{Q(i-1)}$ is the volume of water in the quick flow reservoir at the end of the previous step (mm) and $Q_{Q(i)}$ is the discharge from the quick flow reservoir (mm/day). Lastly, spring discharge (mm/day) was calculated as the sum of quick flow, epikarst, and phreatic discharge to the conduit/spring:

$$Q_{spring(i)} = Q_{Q(i)} + Q_{E(i)} + Q_{P(i)}, \quad (7)$$

The mass balance of solutes (i.e., NO_3^- , NH_4^+ , and DON) within the soil reservoir was modeled as

$$M_{S(i)} = M_{S(i-1)} + (C_{R(i)} R_{(i)} (1-X) - C_{CRCK(i)} Q_{stream(i)} - C_{S(i-1)} Q_{soil(i)} \pm M_{FATE(i)}) \Delta t, \quad (8)$$

where $M_{S(i-1)}$ is the mass of solute in the soil reservoir at end of the previous time step (mg), $C_{R(i)}$ is the seasonal concentration recharging the soil (mg/L) which represents the bulk recharge of many contaminant sources (e.g., precipitation, fertilizer, manure, and sewage), $C_{CRCK(i)}$ is the concentration of the runoff and lateral flow mixture that discharges into the surface stream and is described further in the next paragraph (mg/L), $C_{S(i-1)}$ is the solute concentration of the soil reservoir at the end of the previous time step (mg/L), and $M_{FATE(i)}$ represents biogeochemical mass changes (mg/day) as a function of temperature, a first-order rate constant, and mass of solute. The biogeochemical mass changes (nitrification, mineralization, and denitrification) were modeled as

$$M_{FATE(i)} = M_{S(i-1)} \times k_{ref} \times \theta^{(T_{S(i)} - T_{ref})}, \quad (9)$$

where k_{ref} is a first-order rate constant for a reaction (i.e., k_{DEN} , k_{NITR} , and k_{MIN}) at the reference temperature (day^{-1}), θ is a temperature adjustment coefficient, $T_{S(i)}$ is the soil temperature ($^{\circ}\text{C}$), and T_{ref} is a reference temperature for the reaction ($^{\circ}\text{C}$). This formulation is consistent with the influence of temperature on the rates of the biochemical transformations modeled in this study (Bowie et al., 1985; Reichstein et al., 2000). The epikarst and phreatic zone solute balances are constructed in the same way, whereas solutes in the quick flow reservoir were assumed conservative due to their short residence times. Residence time of water within each reservoir was modeled using a mass balance of water age with recharge to the soil providing “young” or “new” water and subsequent discharge exporting well-mixed reservoir water.

Surface stream NO_3^- concentration is considered as a mixture of low-concentration runoff (i.e., recent recharge) and high-concentration soil water. This end-member mixture is recognized as an important aspect of solute delivery to the in-stream environment (Miller et al., 2017) and was modeled as

$$C_{CRCK(i)} = x_{SOIL} C_{S(i-1)} + x_{REC} C_{R(i)}, \quad (10)$$

where x_{SOIL} is the fraction of stream water of soil origin, $C_{S(i-1)}$ is the soil solute concentration (mg/L), x_{REC} is the fraction of stream water of runoff origin, and $C_{R(i)}$ is the recharge solute concentration (mg/L). In the event that the model produces flow in the surface channel, $C_{CRCK(i)}$ is used as the concentration of recharge to the quick flow aquifer (i.e., stream abstraction); otherwise, the bulk $C_{R(i)}$ value is used and represents recharge into sinkholes and other upland, nonstream karst features.

Lastly, the concentration of solute at the spring (C_{RYSF}) was modeled as

$$C_{RYSF(i)} = (Q_{Q(i)} C_{Q(i)} + Q_{E(i)} C_{E(i)} + Q_{P(i)} C_{P(i)}) / (Q_{Q(i)} + Q_{E(i)} + Q_{P(i)}), \quad (11)$$

where $C_{Q(i)}$ is the concentration of solute in quick flow (mg/L), $C_{E(i)}$ is the solute concentration in the epikarst (mg/L), and $C_{P(i)}$ is the concentration of solute in the phreatic zone (mg/L).

2.1.4. Model Inputs, Parameters, and Evaluation

Four years (2012–2016) of NO_3^- data were collected at the surface stream (CRCK) and subsurface conduit (KYHP) locations. The temporal scale of sampling varied from hourly to biweekly depending on flow

Table 2
Hydrologic and Nitrogen Model Inputs and Parameters

Symbol	Description	Median Value	Parameter Variability	Units	Source
Model inputs					
Δt	Temporal step	1		day	User input
A	Recharge area	5.8×10^7		m^2	Measured in field
α_1	Recession coefficient—quick flow	0.50		day^{-1}	Master recession curve
α_2	Recession coefficient—intermediate flow	0.15		day^{-1}	
α_3	Recession coefficient—slow flow	0.05		day^{-1}	
x_{SOIL}	Fraction of stream water of soil origin	0.25		-	Buda & DeWalle (2009) and Long (2009)
x_{REC}	Fraction of stream water of runoff origin	0.75		-	
$C_{NH_4^+(R)}$	NH_4^+ concentration of recharge	0.12		mg N/L	Measured in field
$C_{DON(R)}$	DON concentration of recharge	0.35		mg N/L	Measured in field
Hydrologic model parameters					
X	Fraction of rain as concentrated recharge	0.05	0.01–0.10	-	Minimum and maximum bounds represent inferred physical bounds.
k_{soil}	Soil percolation coefficient	0.03	0.01–0.11	day^{-1}	
k_{stream}	Soil lateral flow coefficient	1.07	0.11–3.72	day^{-1}	
k_{EL}	Epikarst percolation coefficient	0.04	0.01–0.14	day^{-1}	
Q_{PUMP}	Aquifer pumping rate	0.80	0.32–2.79	mm/day	
$V_{S, MIN}$	Soil field capacity	72.7	16.4–98.2	mm	
$V_{S, MAX}$	Soil height to activate lateral flow	160.6	102–199	mm	
$V_{E, FAST}$	Height to activate quick epikarst pathway	15.9	1.85–46.8	mm	
Nitrogen model parameters					
$C_{NO_3^-(F)}$	NO_3^- concentration of fall recharge	2.75	1.30–3.90	mg N/L	Bound by minimum and maximum values of observed stream data
$C_{NO_3^-(W)}$	NO_3^- concentration of winter recharge	2.73	1.40–3.90	mg N/L	
$C_{NO_3^-(SP)}$	NO_3^- concentration of spring recharge	0.52	0.02–1.62	mg N/L	
$C_{NO_3^-(SU)}$	NO_3^- concentration of summer recharge	0.86	0.08–2.15	mg N/L	
k_{DEN}	Denitrification first-order rate constant	0.005	0.001–0.015	day^{-1}	Bound by literature-derived rates (Bowie et al., 1985; Tesoriero & Puckett, 2011)
k_{NITR}	Nitrification first-order rate constant	0.205	0.065–0.481	day^{-1}	
k_{MIN}	Mineralization first-order rate constant	0.028	0.013–0.078	day^{-1}	

Note. Each input and parameter is presented with a description, measured or calibrated value, parameter variability remaining after uncertainty analysis, units of measurement, and the source material for the input or parameter.

conditions (i.e., baseflow versus flood conditions). In the field, surface stream samples were collected using 1-L HDPE bottles with either manual collection or an automatic sampler (ISCO 6712) depending on flow conditions. For the subsurface conduit, a bailer with a one-way check valve was used to ensure that well samples were collected at the depth of the conduit. The Kentucky Geological Survey laboratory analyzed NO_3^- samples, consistent with U.S. EPA Method 300.0, using a Dionex ICS-3000 Ion Chromatography System featuring a carbonate–bicarbonate eluent generator and Dionex AS4A analytical column. The NO_3^- anion was identified by retention time and the peak area was compared to a calibration curve generated from known standards. QAQC protocol included (i) analyses of NIST secondary source standards before and after each run to verify calibration, (ii) blanks before and after each run to verify lack of carry-over in the column, and (iii) analyses of randomly selected duplicate samples to verify that deviation was less than 10%. Field ($n = 8$) and lab ($n = 49$) duplicates of NO_3^- had a standard deviation of 0.07 and 0.02 mg N/L, respectively. No field or lab blanks registered above the method detection limit. Failure of any criteria involved the researchers questioning the protocol and rerunning the batch. Previously collected ammonium (NH_4^+) and dissolved organic N (DON) data were used to estimate NH_4^+ and DON concentrations of recharge to the watershed (Table 2). The recharge concentration of NH_4^+ ($C_{NH_4^+(R)}$) was fixed as a constant (mean: 0.12 ± 0.19 mg N/L; $n = 54$) as field-collected data were not available over the same time scales and at the same spatial locations as the primary NO_3^- data set (Kentucky Water Watch (KWW), 2016). Additionally, NH_4^+ concentrations were 1 to 2 orders of magnitude less than NO_3^- concentrations. Likewise, the recharge concentration of DON ($C_{DON(R)}$) was also assumed constant (mean: 0.35 ± 0.07 mg N/L; $n = 4$) for the same reasons as NH_4^+ (UKCAFE, 2011).

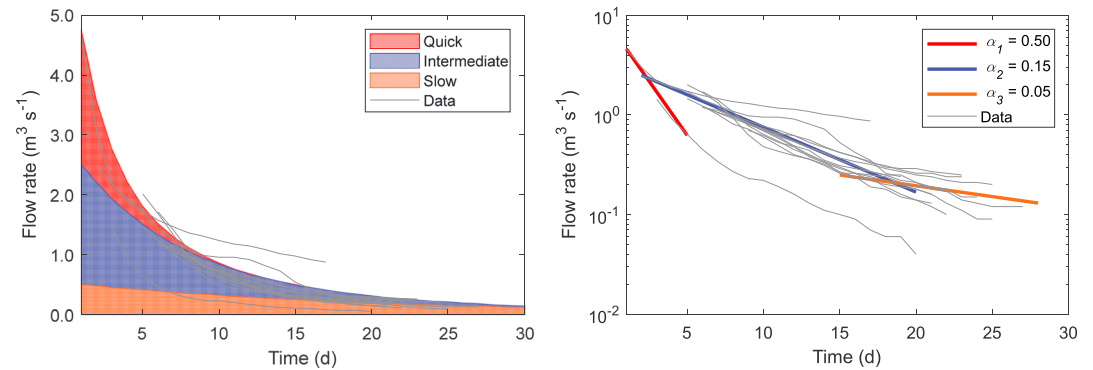


Figure 4. Master recession curve (MRC) for Royal Spring using 13 events over two decades of flow data. The MRC was decomposed into three constituent reservoirs (quick, intermediate, slow) and recession coefficients (α_1 , α_2 , α_3) were fitted to match data results (see Malík & Vojtková, 2012).

Recession coefficients were estimated from a master recession curve constructed using 13 events over two decades (Figure 4). The recession coefficients show some variation from storm-to-storm as the storms occurred under varying hydrologic conditions and over multiple decades (e.g., wet season versus dry season, high versus low antecedent conditions, large events versus small events). The fractions of stream water from soil and runoff origin can vary from event to event, but were selected in this study based on a range of values reported in the literature for karst using isotopic hydrograph separation (Buda & DeWalle, 2009) and two-domain modeling (Long, 2009). Surface events in the Cane Run Watershed are short-lived and often peak and recede within a day (i.e., the time step of the model; Husic, Fox, Agouridis, et al., 2017), providing support that an average value for the respective soil and runoff fractions can adequately portray mixing processes. Hydrologic model parameter sets were generated and evaluated over a wide range of values. Minimum and maximum values were selected to represent inferred physical bounds. For example, the soil percolation coefficient is bounded on the high end by the coefficient for quick flow and on the low end by “0” (i.e., no flow). The seasonal NO_3^- concentration of recharge water was varied over the minimum and maximum values of observed stream NO_3^- data, using Monte Carlo sampling and assuming a uniform distribution. The upper limits for biogeochemical first-order rate reactions were estimated using values based on temperature (Table 2 for references).

The framework for evaluating model performance includes the generation of a set of model parameters, comparison to measured data, and the evaluation against statistical criteria (Figure 5). The calibration objective for the hydrologic model was mean daily spring discharge. For simulations satisfying the calibration objective, an additional test against three “soft rules” for hydrologic process or “behavioral” representation was performed, similar to other karst studies (Hartmann, 2017; Sarrazin et al., 2018), including representation of streamflow, evapotranspiration, and pumping abstractions. Based on previous field investigation, 25% of water outputs are discharged as streamflow (Husic, Fox, Agouridis, et al., 2017), 60% of precipitation is lost to evapotranspiration (Hanson, 1991), and 15% of total streamflow is removed by water-treatment plant and farmers (Kentucky Geological Survey and Georgetown Municipal Water and Wastewater Service personal communication, 2016). An uncertainty bound of $\pm 10\%$ is attached to each of these three rules. We discretize process representation into three bins. “LOW,” “MED,” and “HIGH” indicate that <33%, 33–66%, and >66%, respectively, of acceptable model runs (i.e., those that satisfy the objective function) also adequately represented the water balance behavior. A LOW performance by a model structure in any of the three soft rules removes the model from consideration because the structure does not come close to reflecting real system processes.

The hydrologic ($n = 1,461$) and NO_3^- ($n = 162$) data sets were divided into calibration and validation subsets of equal cardinality. Split sample subsets were selected for the hydrologic model evaluation with the first two years used as calibration and the last two years used as validation. Evaluation subsets for the N model were randomly selected for each model realization as the frequency of NO_3^- data collection varied over the four-year period and split sampling would have biased the model to time periods with greater density of collected

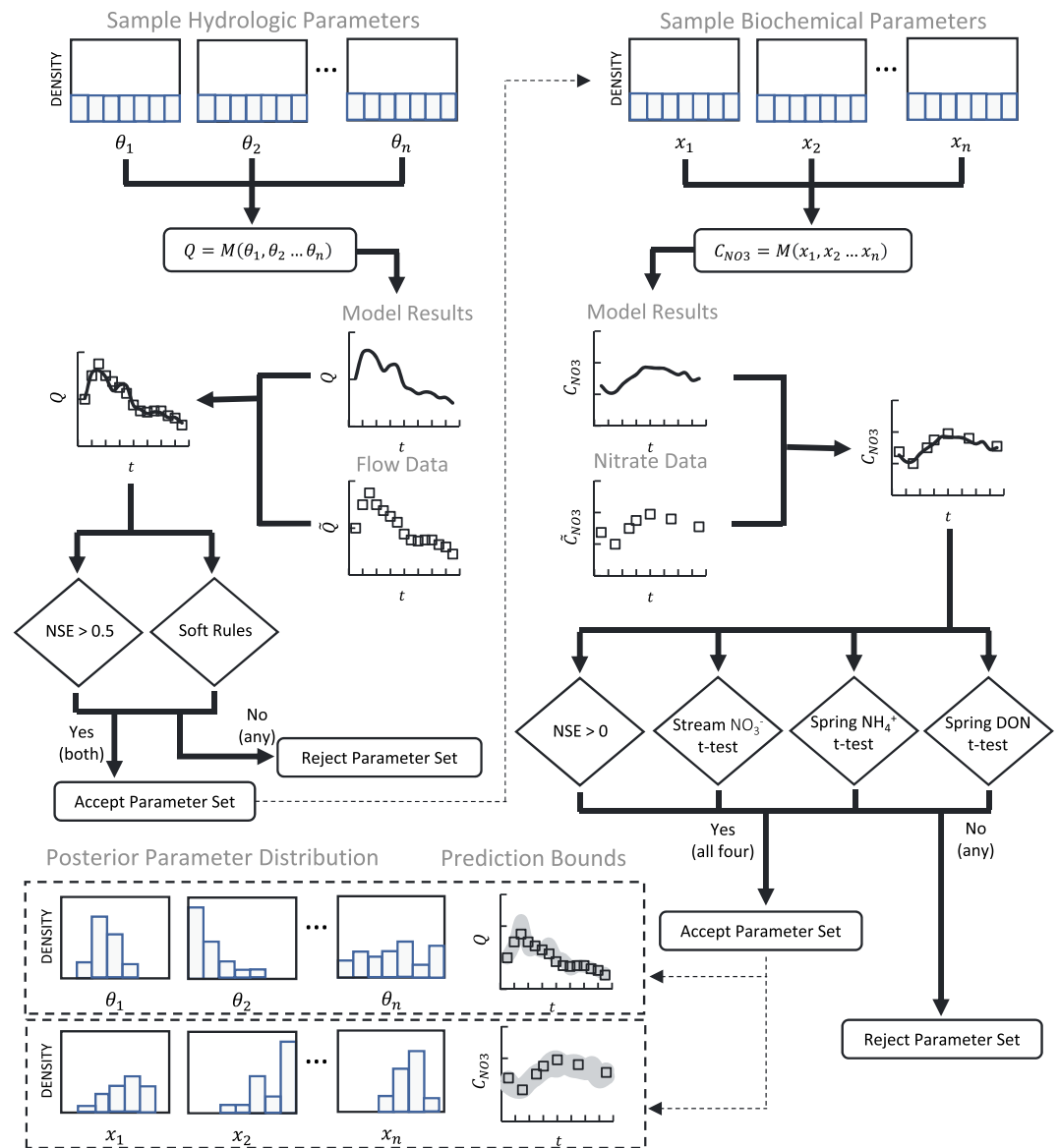


Figure 5. Framework for evaluating hydrologic and nitrogen model uncertainty in parameters and predictions. Hydrologic model parameters (θ) are sampled from an assumed prior distribution. The parameters are fed into the numerical model, M , and simulated model results (Q) are compared to measured flow data (\bar{Q}). Only model realizations and parameter sets that satisfy the objective function and three “soft rules” (see section 2 for explanation) are retained. Accepted hydrologic parameter sets are fed through to the dissolved nitrogen model where biochemical parameters (x) are sampled and model results (C_{NO_3}) are evaluated against measured spring data (\bar{C}_{NO_3}). Evaluation statistics for the dissolved nitrogen model include a Nash-Sutcliffe efficiency (NSE) function for spring NO_3^- results and t tests for modeled versus measured means of stream NO_3^- , spring NH_4^+ , and spring DON. Lastly, accepted hydrologic and biochemical realizations are used to construct posterior parameter distributions and prediction bounds.

data (Liu et al., 2018). Initial model conditions were selected based on mean model results, but typically initial conditions in karst have little effect on evaluation statistics if the model is initiated during very low water periods and the upper reservoirs are disconnected from the lower (Mazzilli et al., 2012). Both conditions were satisfied in this study.

The Nash-Sutcliffe efficiency (NSE) was selected as the statistical evaluation metric due to its ubiquitous use in hydrologic modeling and established performance guidelines (Moriiasi et al., 2007). The NSE statistic was calculated as

$$\text{NSE} = 1 - \frac{\sum_{t=1}^T (N_m^{(t)} - N_o^{(t)})^2}{\sum_{t=1}^T (N_m^{(t)} - \bar{N}_o)^2}, \quad (12)$$

where T is the total number of observations, $N_o^{(t)}$ is the observed value for sample t , $N_m^{(t)}$ is the modeled value for sample t , and \bar{N}_o is the mean of all observed values. The Nash-Sutcliffe efficiency ranges from $-\infty$ to 1, with 1 indicating a perfect match of the model to data and 0 indicating that the model performs no better than the mean of the data (Moriassi et al., 2007). We also calculate the NSE for high flows (top 20% of discharge time series) and low flows (remaining 80%) (Hartmann et al., 2013). Considering the criteria set out by Moriassi et al. (2007), minimum NSE values of 0.5 and 0 were set for spring discharge and spring NO_3^- concentration results, respectively. Minimum criteria for the hydrologic model evaluation are commonly reported (e.g., Moriassi et al. (2007) recommends 0.5), but there are a lack of accepted thresholds for NO_3^- performance so the authors impose a rule on the model that it must perform at least as well a NSE of 0 (i.e., the model has at least some predictive strength). The use of NO_3^- concentration rather than NO_3^- flux to calibrate the N model is more difficult but was performed for two reasons. First, NO_3^- flux statistics are highly correlated with discharge and lead to biased water quality model performance (Hirsch, 2014). Second, calibrating to concentration rather than flux gives a more accurate description of internal watershed N cycling. The accepted spring NO_3^- solution space was further constrained so that modeled stream NO_3^- , spring NH_4^+ , and spring DON results were not statistically different ($\alpha = 0.05$, using Welch's t test) from observed stream NO_3^- (mean: 1.92 ± 1.02 mg N/L; $n = 111$), spring NH_4^+ (mean: 0.07 ± 0.11 mg N/L; $n = 40$), and spring DON (mean: 0.23 ± 0.14 mg N/L; $n = 19$) data (Kentucky Geological Survey (KGS), 2018). Only samples collected while water was moving (i.e., no standing water) were included in model evaluation as standing water samples are potentially influenced by nonsubsurface karst cycling, such as uptake/growth processes between the spring mouth and the sampling location, which are not representative of upstream karst pathways or processes.

Numerical modeling uncertainty analysis was performed on an institutionally shared high-performance computing cluster (DLX2/3) with 4800 processor cores, 18 TB of RAM, and 1 PB of high-speed disk storage. Uncertainty in the hydrologic and N models was assessed with the generalized likelihood uncertainty estimation method (Figure 5), which has been applied to water resources modeling to assess the equifinality of model parameter sets (Beven, 2006; Ford et al., 2017). The generalized likelihood uncertainty estimation methodology is initiated by assuming a prior distribution (e.g., uniform) for model parameters. Parameter sets that satisfy one or more evaluation statistics are retained while sets that fail are discarded. A posterior distribution is then constructed from the collection of acceptable sets. A prediction bound can also be used to represent water and NO_3^- results that are contained by 95% of accepted simulation results. In this study, several hundred acceptable hydrologic parameter sets were first established requiring millions of simulations. Thereafter, they were randomly fed through to the N model where several hundred more parameter sets were deemed acceptable requiring millions more simulations. The final NO_3^- prediction bounds represent both the effects of physical (water) and biochemical (N) uncertainty.

2.2. Karst Pathways, Processes, and Timing of N Transport

2.2.1. Pathways Controlling N Transport

Pathways controlling N transport were investigated using residence time and correlation analyses of both data and numerical model results. Autocorrelation and cross-covariance are two methods by which water pathways and residence time can be better understood for assessing N fate. The autocorrelation function indicates the memory effect of the system, and a predetermined value of 0.2 is typically used to represent the decorrelation lag time (Mangin, 1984). Cross-covariance can indicate the relationship between an uncorrelated cause (e.g., rainfall) and the subsequent effect (e.g., spring discharge; Kovačič, 2010). Pathways controlling N transport were also quantified using integration of numerical modeling results. Each flow path (quick flow, epikarst, and phreatic) was integrated with a daily time step over the model simulation to estimate total pathway load. Model integrated budgets could be compared across pathways to indicate the relative importance of certain pathways on controlling N transport.

2.2.2. Processes Affecting N Exports

The physical and biochemical processes impacting N exports from karst were investigated. An N budget of physical processes such inflows (diffuse infiltration and concentrated recharge) and outflows (karst spring,

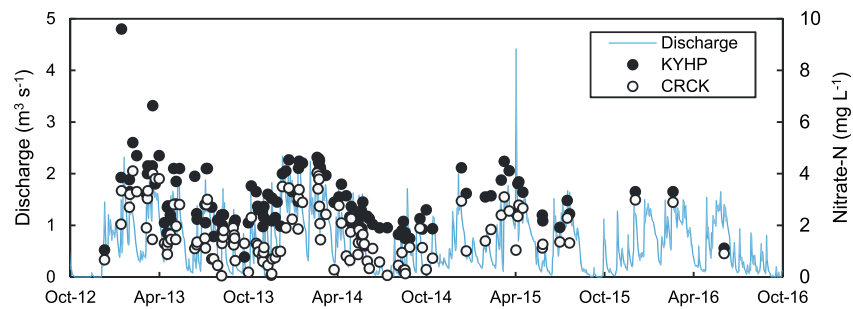


Figure 6. Concurrently sampled surface stream (CRCK) and subsurface phreatic conduit (KYHP) NO_3^- concentrations ($n = 99$) shown alongside spring (RYSP) discharge.

surface stream, and net aquifer losses such as pumping) were constructed. A similar budget of biogeochemical N processes (denitrification, nitrification, and mineralization) was performed within each reservoir and the watershed as a whole. Physical processes such as soil-epikarst connectivity (depending on field capacity of soil) may act to retain and accumulate NO_3^- in the soil prior to subsequent leaching during hydrologic activity. Other processes such as evapotranspiration affect both the water budget and the N concentration within the soil reservoir. The temporal distribution of these processes was of note, considering that they may be impacted by daily or seasonal variations in temperature, humidity, sunlight, N source, soil moisture, and aquifer abstractions. The distribution of these processes across the multiple storage zones was also of interest, and solute concentrations were compared across pathways over several years to estimate processes affecting N exports.

2.2.3. Timing of N Exports From Karst

Timing of N exports from karst was analyzed to assess temporal delivery of NO_3^- to downstream waterbodies. We performed an analysis using results from a recent fluvial-dominated, immature karst study in Ford et al. (2017) to provide comparison with karst-dominated NO_3^- results from the present system. The South Elkhorn (62 km²) drains southwest Lexington, KY, while the Cane Run system (58 km²) drains the northern portion of the city. The distribution of land uses, soil conditions, and topography are nearly identical in the two systems. However, Cane Run is underlain by mature karst topography that includes fractures, sinkholes, swallets, and conduits forming the Royal Spring groundwater basin, whereas the South Elkhorn has weak karst development and perennial surface streamflow (Mahoney, Al Aamery, et al., 2018; Mahoney, Fox, et al., 2018). Both systems drain to Elkhorn Creek, and then to the Kentucky, Ohio, and Mississippi Rivers. Nitrogen loading from the South Elkhorn was produced using results in Ford et al. (2017) at the single watershed outlet. Results for N loading from the Cane Run-Royal Spring system was produced by summing loads from both the surface stream and conduit outlets from the watersheds in order to provide an integrated watershed response. The temporal distribution of N loading to downstream waterbodies was then analyzed graphically, and comparisons were made between the karst-dominated drainage and the nonkarst system.

3. Results and Discussion

3.1. Numerical Model Development and Application

Prior to assessing the numerical model, we first investigate trends in collected data. Results of N seasonality in water, comparison of surface and subsurface N concentrations, and N dynamics during storms were generally consistent with existing data. The sinusoidal pattern in NO_3^- concentration at both locations (Figure 6) reflects the seasonality of anthropogenic loading, soil processes, and hydrologic mobilization of N. The agricultural land use and temperate climate, including fall and winter application of fertilizer (UKCAFE, 2011), dormancy of vegetation, and hydrologic mobilization, coincides with seasonal N levels. These results are typical of agricultural watersheds where overapplication of fertilizer and manure during the fall, coupled with mobilization of accumulated N, can lead to excess runoff and leaching of NO_3^- in winter (Royer et al., 2006; Toran & White, 2005). Nitrate concentrations of samples collected on the same day at both sites are ~50% greater in the karst conduit than the surface stream (Figure 6). Further, 95 of the 99 paired daily-averaged samples show greater NO_3^- concentrations in the subsurface. This result is consistent with agricultural landscape processes such as soil N accumulation followed by hydrologic N mobilization of

Table 3
Hydrologic and Nitrogen Model Evaluation Results

Description	Model 1	Model 2	Model 3a	Model 3b	Model 4a	Model 4b	Model Evaluation Comments
Hydrologic model evaluation							
Model calibration (NSE)	0.59	0.59		0.58		0.63	Slight differences between models. Model 4 was the only structure with an NSE > 0.60 and it has the most data-derived parameters.
Model validation (NSE)	0.47	0.45		0.43		0.44	
Average high-flow skill (NSE)	0.31	0.35		0.24		0.29	
Average low-flow skill (NSE)	0.63	0.61		0.60		0.60	
No. of free water parameters	5	6		6		8	
No. of data-derived parameters	0	1		2		3	
Representation of processes							
Representation of streamflow (15–35% of total outflow)	MED	HIGH		LOW		MED	Only Model 4 successfully simulated all <i>streamflow</i> , <i>evapotranspiration</i> , and <i>pumping</i> representations.
Representation of evapotranspiration (50–70% of recharge)	LOW	LOW		MED		MED	
Representation of pumping (5–25% of recharge)	MED	MED		HIGH		HIGH	
Nitrogen model evaluation							
Model skill—calibration (NSE)	0.30	0.33	0.38	0.40	0.40	0.46	N model metrics improved with more reservoirs. Model 4a has <i>improved performance</i> over Models 1, 2, 3a, and 3b and <i>fewer parameters</i> than 4b.
Model skill—validation (NSE)	0.10	0.11	0.03	0.11	0.15	0.05	
No. of free nitrogen parameters	7	7	7	10	7	13	

Note. Tested model structures range from one to four reservoirs (Figure S1). Models 3 and 4 have *a* and *b* subsets. Subscript *a* indicates global nitrogen first-order rates, whereas *b* indicates reaction rates unique to each reservoir. Evaluation metrics include the Nash-Sutcliffe efficiency (NSE) statistic, performance during high- and low-flow periods, number of free and data-derived parameters, and representation of processes. Model 4a was chosen as the optimal model structure when considering performance, parameter identifiability, and process representation.

highly concentrated subsurface water (Di & Cameron, 2002). It is also consistent with biotic uptake, which can cause lower N concentrations in agriculturally impacted surface streams (Birgand et al., 2007; Mulholland et al., 2008). Lastly, the timing of NO_3^- concentration peaks caused by storm events and seasonality are well matched by the surface and subsurface pathways (Figure 6). The result demonstrates the pressure pulse of stormflow on the karst subsurface that can mirror the temporal response seen in surface streams (Husic, Fox, Agouridis, et al., 2017). Further, the multiple inferred pathways (i.e., quick flow, epikarst, and phreatic) introduce wide temporal variability in NO_3^- data results. In many instances, the NO_3^- concentration of samples collected from the spring within days of one another (e.g., see April 2013 in Figure 6) can span over 3 mg N/L, highlighting the influence of pathway variability on spring NO_3^- concentration. The N export behavior in this karst system tends to agree with the hypothesis that precipitation can dominate interannual variability of downstream N loading (Sinha & Michalak, 2016). Data results of NO_3^- at the surface stream and karst spring provided the basis for our numerical model evaluation.

Evaluation of the various model structures for hydrologic and N simulation in karst suggested that a four-reservoir model (soil, quick flow, epikarst, and phreatic) was the most appropriate for the Cane Run watershed (Table 3). While there were only slight differences in the calibration and validation statistics across model structures, the four-reservoir model was the only model that successfully simulated the behavioral processes of streamflow, evapotranspiration, and pumping. Therefore, the four-reservoir model was selected for simulation of hydrology and N fate in our karst system. The water component of the numerical model produced satisfactory results throughout the four-year simulation period (Figure 7a). Baseflow conditions were well-represented by the model during both the active winter and dryer summer periods, which reflects the model's ability to accurately represent subsurface water storage and drainage. The satisfactory simulation of spring flow recession following hydrologic activity provides support for the master recession curve analysis (Figure 4) used to estimate recession coefficients. Peak flows were adequately simulated, although not as well as baseflow, by the model and represented pulses of discharge occurring primarily via quick flow pathways. High flows are typically more difficult to model as the high spatiotemporal variability of rainfall, routing, and intermittent storage introduces complexity to the flow routing process (Moriasi et al., 2012). Successful performance of the parent water model gave us confidence in carrying the results forward to the N fate subroutines.

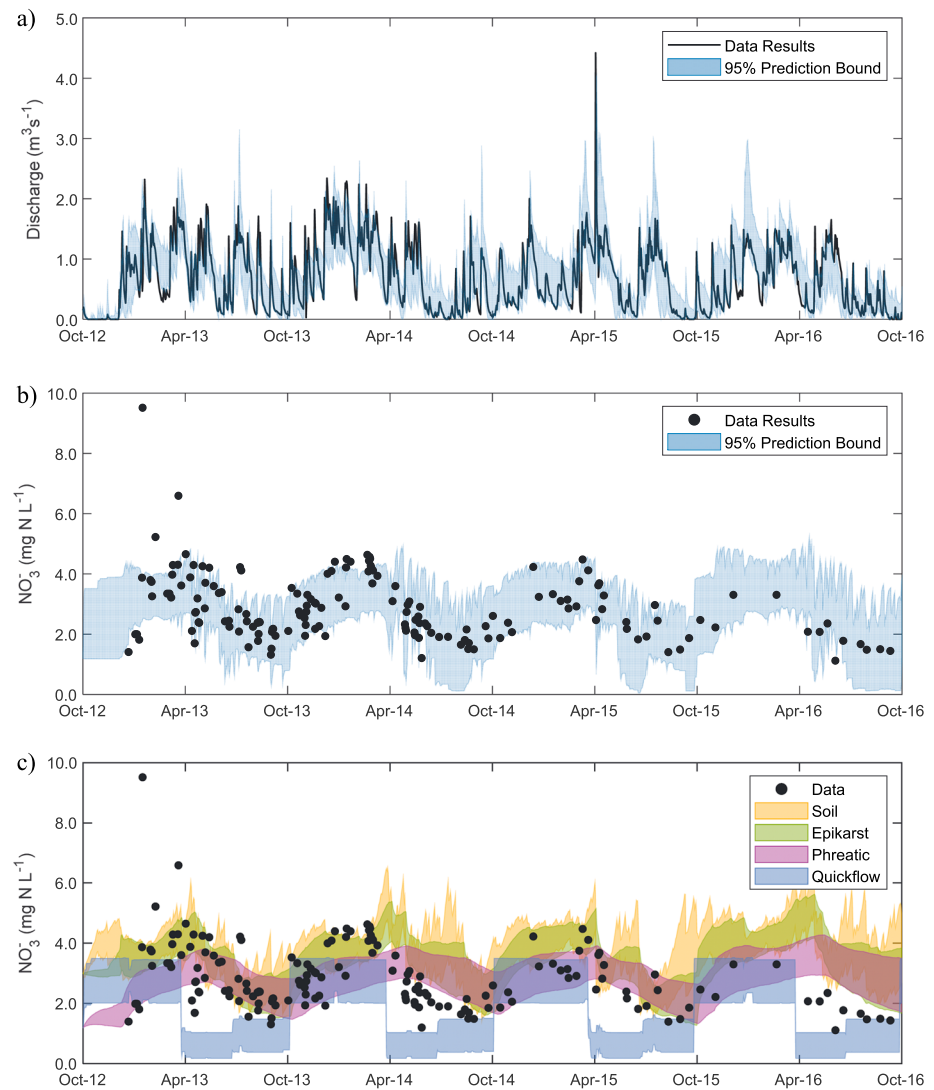


Figure 7. (a) Hydrologic model results simulating Royal Spring discharge. (b) Nitrogen model results simulating NO_3^- concentration at Royal Spring. (c) NO_3^- concentration within the four modeled reservoir pathways. Prediction bounds for each pathway include 66% of accepted results—rather than 95%—for visual clarity of the differences in mean pathway concentrations.

For N fate and transport, we also tested multiple model structures and conclude that the four-reservoir model with global N parameterization is the optimal structure because of its improved performance and parsimony (Table 3). Numerical model results of N fate and transport reflect NO_3^- seasonality and storm event dynamics (Figure 7b). The model performed very well with 123 of the 164 NO_3^- data results (75%) falling within the modeled prediction bounds. Model bounds are wide as biochemical uncertainty is also affected by hydrologic uncertainty in the parent model. For example, transitions from quick flow to epikarst flow control of spring discharge can substantially impact NO_3^- concentration as the two flow paths may have significantly different solute signatures (Figure 7c). Still there could be external processes not included in the model that may limit the percentage of results contained within the uncertainty bounds. However, our use of discharge and NO_3^- coincides with the most informative data streams as identified in other karst studies (e.g., Hartmann et al., 2017). Modeled subsurface NO_3^- concentration remains elevated throughout the spring season despite a decrease in seasonal NO_3^- recharge from the surface indicating storage and release of high concentration NO_3^- (see Figure 7c). Quick flow shows a step-like behavior because NO_3^- recharge in the basin was modeled using a piecewise equation based on seasonality. Our statistical results

for N modeling were good (Table 3), which offers confidence to the multireservoir approach as a tool for modeling NO_3^- . In particular, model performance is impressive given the time scale and response variable used for model evaluation (i.e., daily N concentration rather than daily, weekly, or monthly N load/yield). Evaluation statistics are recognized to decrease as time frequency of model evaluation increases (Yuan et al., 2001) and when concentration rather than load is used as the response variable (Hirsch, 2014). The N model developed in this study accurately portrays watershed N dynamics and is capable of successfully simulating daily NO_3^- concentration at the primary karst springhead.

Our uncertainty analysis with the high-performance computer was pivotal to constraining and bounding reservoir model results. For the hydrologic model, 1,560,000 model realizations were performed, of which 3,653 were successful. For the N model, 30,072,000 model realizations were performed, of which 1,382 were successful. If the uncertainty analysis were performed on a single machine, it would have taken over 200 days in simulation time, but that was cut down to just 1.5 days as the simulations were distributed over 164 cores on the high-performance cluster. A large number of model simulations were necessary for a few reasons: the physical and biochemical parameter bounds were wide to encompass potential equifinality as well as provide a conservative estimate of modeled processes; each biochemical parameter set was generated and then applied randomly to an accepted hydrologic parameter sets—recognizing the equifinality that may occur not only in one submodel but also its parent model; and finally, failure of any one of the multiple calibration objectives resulted in the entire parameter set being discarded (see Figure 5). To that last point, the three soft water rules and four N calibration objectives—spring NO_3^- , stream NO_3^- , spring NH_4^+ , and spring DON—had success rates of approximately 20%, 2%, 15%, 30%, and 20%, respectively, per model realization. Taken together, if the respective success rates are uncorrelated, the composite success rate for any random realization was 0.004%. The use of high-performance computing was instrumental to running the required number of simulations necessary to build a posterior sample distribution, construct a prediction bound, and evaluate uncertainty within multiple submodels.

Calibration to nitrogen data and the use of soft rules for behavioral process representation also decreased equifinality in discharge estimates by reducing the number of acceptable hydrologic parameter sets from 3,653 to 419 (an 89% reduction). The reduction in equifinality by including the N model and rules for process representation had material effects when inferring water pathway results. For example, from the original 3,653 parameter sets, 46% of the water was discharged by epikarst, 32% by the phreatic zone, and 22% by quick flow. However, by including only hydrologic sets that also produce satisfactory N model results and represent behavior processes, the remaining sets ($n = 419$) indicate that 42% of water is discharged by epikarst, 39% by phreatic zone, and 19% by quick flow. The utility of multiple response variables to reduce equifinality has been noted in other systems such as in surface streams using stable isotopes (Ford et al., 2017; Ford & Fox, 2015), in watershed-scale models using remote-sensing data (Silvestro et al., 2015), and in vegetation zones using carbon data representative of different time scales (Carvalho et al., 2010). We add to this list with an application of equifinality reduction to water flow dynamics in an agricultural karst system using an N data set and numerical modeling.

Uncertainty analysis indicated that some hydrologic model parameters vary considerably from the assumed uniform prior distribution to the posterior distribution (e.g., k_{soil} and X ; Figure 8a). Two posterior distributions are shown: *a* and *b*. “Posterior *a*” results show the hydrologic parameter distributions *before* including the soft rules or N data. “Posterior *b*” results highlight the distribution of hydrologic parameters *after* including the soft rules and N data. Primarily, the inclusion of the soft rules and N data act to shift the parameter distributions toward increased residence time in the soil (see decreases in k_{soil} and k_{stream} , but increases in $V_{S, MIN}$ and $V_{S, MAX}$). These changes reflect the model constrains of reconstructing the water balance, where the two outputs are primarily the stream and subsurface spring, and allowing for a long enough residence time to transform stored N. The sensitivity in the fraction of rainfall redirected as concentrated recharge to the conduit (X) was important in simulating peaks in the spring flow hydrograph. Uncertainty analysis for the biochemical transformation rates of NH_4^+ , DON, and NO_3^- (Figure 8b) indicates an order of magnitude difference in the value of their respective first-order rate constants (note that x axis values are presented as the \log_{10} value of the rate). Results are consistent with existing literature, indicating that NH_4^+ turnover can be quick while substantial NO_3^- denitrification is heavily influenced by residence time (Bowie et al., 1985; Tesoriero & Puckett, 2011). While the first-order rate constants may vary over several orders of

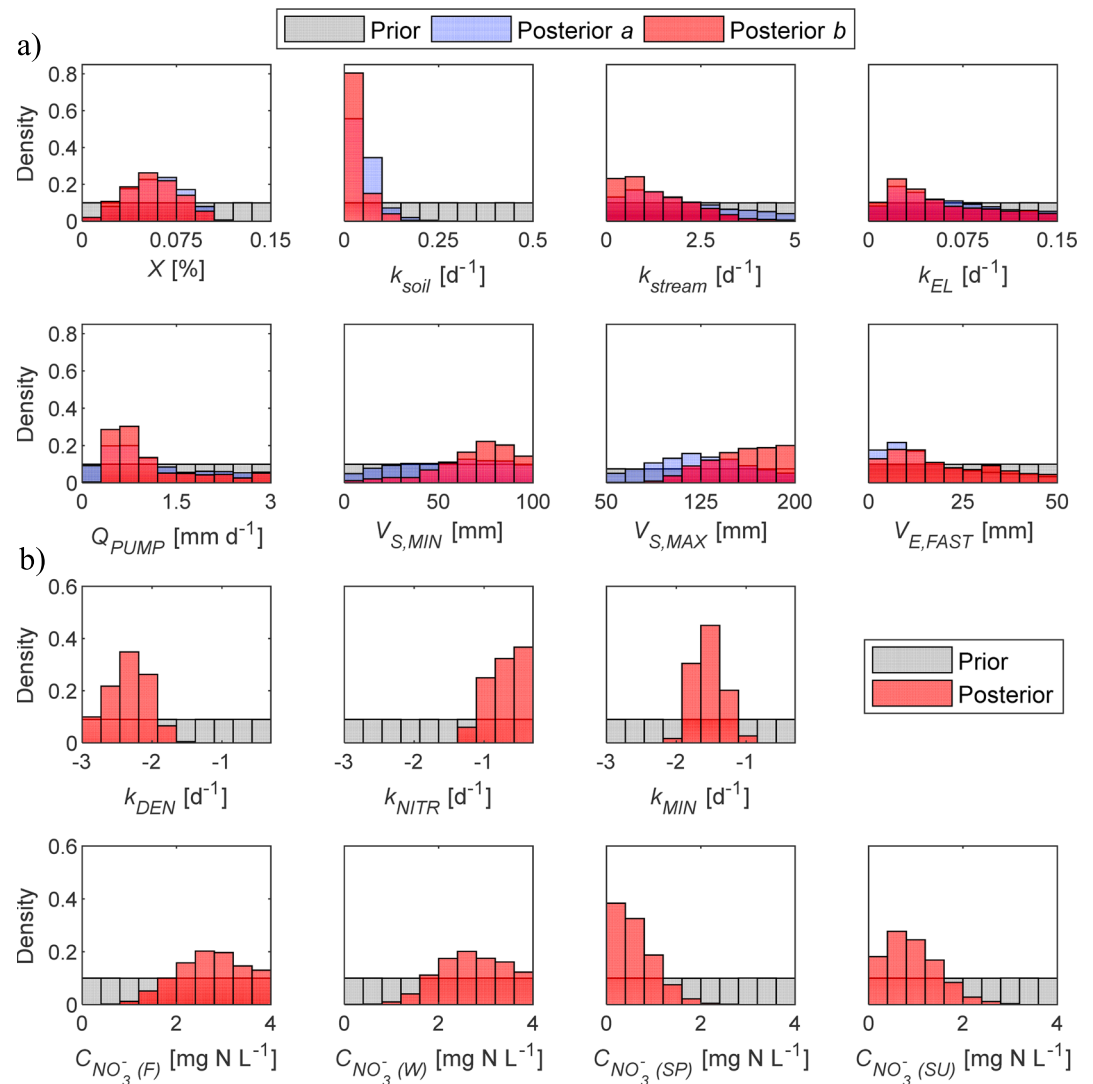


Figure 8. (a) Prior and posterior distributions of hydrologic model parameters: X (concentrated recharge fraction), k_{soil} (soil discharge coefficient), k_{stream} (stream discharge coefficient), k_{EL} (epikarst seepage discharge coefficient), Q_{PUMP} (aquifer pumping rate), $V_{S,MIN}$ (soil field capacity), $V_{S,MAX}$ (soil saturation), and $V_{E,FAST}$ (activation height for fast epikarst pathways). “Posterior a” results show the hydrologic parameter distributions *before* including the soft rules or nitrogen data. “Posterior b” results highlight the distribution of hydrologic parameters *after* including the soft rules and nitrogen data. (b) Prior and posterior distributions of nitrogen model parameters: denitrification (k_{DEN}), nitrification (k_{NITR}), and mineralization (k_{MIN}) first-order rate constants. Also shown are the seasonal NO_3^- concentrations for fall ($C_{NO_3(F)}$), winter ($C_{NO_3(W)}$), spring ($C_{NO_3(SP)}$), and summer ($C_{NO_3(SU)}$) recharge. Note: The x axis for the first-order rates is presented as the \log_{10} value of the rate.

magnitude, their net impact is dependent on the size of the pool that the reactions occur in. Analysis also indicates that fall and winter have the most concentrated NO_3^- recharge to the watershed while spring and summer have the most dilute NO_3^- recharge.

In summary, consistency of the N data set with literature and our numerical modeling results gave us confidence in carrying the model forward to assess pathways, processes, and timing of N in karst. We focused heavily on performing robust uncertainty analysis as only 10% of published water quality modeling papers between 1992 and 2010 ($n = 257$) include any uncertainty analysis (Wellen et al., 2015). Our extensive uncertainty analysis was pivotal to gaining confidence in the N results, and our study details a method for karst researchers who aim to assess hydrologic and biochemical uncertainty in their own models.

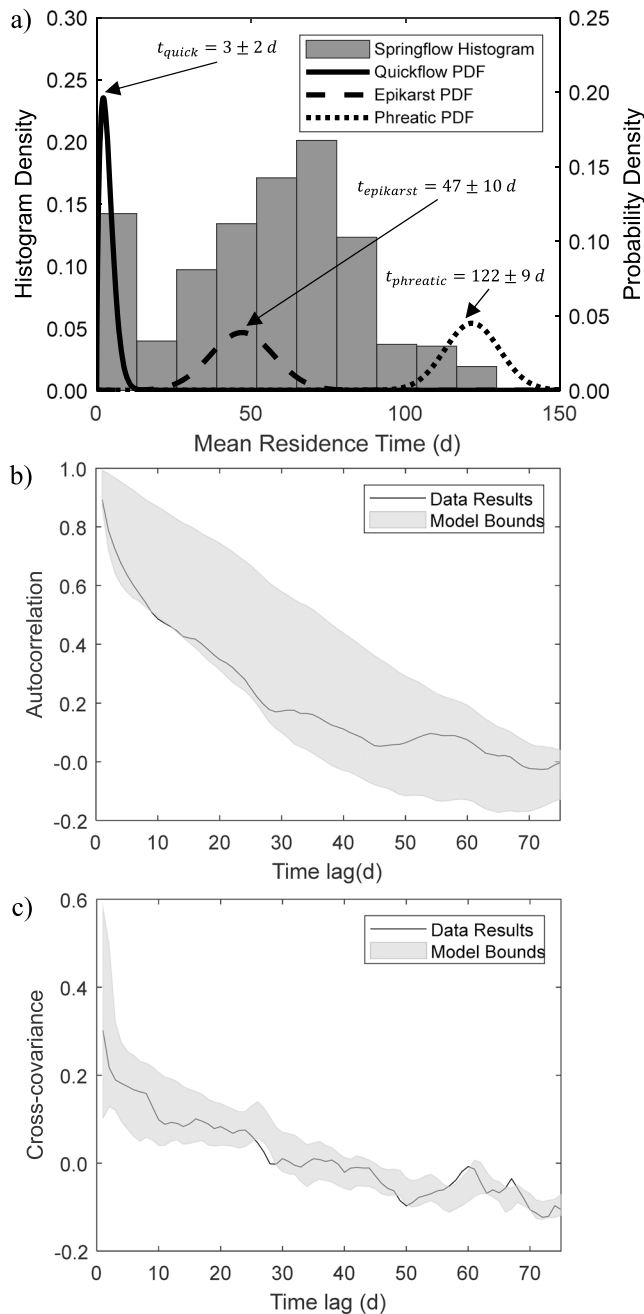


Figure 9. (a) Modeled mean residence time of spring water decomposed into three karst pathways (results presented are from the optimal simulation). (b) Autocorrelation analysis of modeled and measured spring discharge. (c) Cross-covariance analysis of rainfall with modeled and measured spring discharge. Model bounds include 95% of accepted model simulations.

Table 4
Percentages of Water and NO_3^- Yield ($\pm 1\sigma$) From Modeled Karst Pathways

Reservoir	Water Discharged (%)	Nitrate Exported (%)
Quick flow	19 ± 7	11 ± 5
Epikarst Flow	42 ± 22	49 ± 25
Phreatic Flow	39 ± 22	40 ± 26

3.2. Karst Pathways, Processes, and Timing of N Transport

3.2.1. Pathways Controlling N Transport

Residence time results provide a first look at karst pathways controlling N transport. The residence time of spring water spans 3 orders of magnitude (Figure 9a). Quick flow water is discharged on the order of a few days, epikarst water is drained within weeks, and phreatic water is typically exported over several months. The maximum cross-covariance occurs on the same day as rainfall and rapidly decreases thereafter, and both data and model results show similar steepness and decorrelation times (Figures 9b and 9c). The results indicate a pressure pulse of fluid through the system with an immediate response to storm inputs, which is indicative of high karstification. However, results also indicate that distributed recharge is stored within the aquifer and drained by epikarst and phreatic pathways for months to weeks after input. Our residence time results show agreement with water tracing results of others (Bottrel & Atkinson, 1992), and the mean residence time curve agrees with the potential for high-volume water storage in the saturated aquifer (e.g., Knierim et al., 2013).

A water and NO_3^- budget over the four-year observation period shows that epikarst and phreatic pathways contribute, on average, 89% of the annual NO_3^- yield (Table 4). Quick flow in karst aquifers acts to dilute spring NO_3^- concentration with model results indicating that the quick flow pathways compose 19% of total water discharge, but only 11% of the NO_3^- load. On the other hand, the intermediate pathway (i.e., epikarst) sees an increase in the percentage of NO_3^- exported (49% compared to water discharged (42%) while the phreatic pathway has the most similar NO_3^- (40%) and water (39%) yields. The contribution of the three pathways to the N load can also vary temporally from season-to-season and year-to-year (Figure 10). The epikarst N load dominates much of the NO_3^- flux from the spring primarily due to three factors: the epikarst can act as a large storage zone for infiltrated water (Aquilina et al., 2006), the epikarst is well connected to highly concentrated soil water (Fretwell et al., 2005), and the epikarst behaves as a dynamic transfer zone that is effective at conveying water to the spring and conduit via enlarged fractures (Williams, 2008). The quick flow contribution increases at the incidence of hydrologic activity and contributes relatively diluted NO_3^- to the spring flux signal. The long residence time of water in phreatic pores could lead to net denitrification (Heffernan et al., 2012) as pathway results indicate that high NO_3^- concentrations from percolating epikarst water are decreased prior to export by the phreatic pathway.

Our results place emphasis on diffuse (i.e., epikarst and phreatic) pathways when estimating dissolved N fate. Water budget estimates indicate that <6% of recharge is directed to quick flow pathways (Table 5), reinforcing a need to focus on distributed soil recharge even in watersheds heavily influenced by karst topography. Our results are noteworthy because studies often emphasize quick flow contamination of mature karst aquifers via high-speed water and contaminant transport through sinking streams, turbulent conduits, and vertical shafts which preclude aquifer bioremediation (Daly et al., 2002). Quick flow-associated pathways may provide the dominant origin for some contaminants (e.g., sediment-bound contaminants in sinking streams; Husic, Fox, Agouridis, et al., 2017; Husic, Fox, Ford, et al., 2017); however, our results suggest that slow

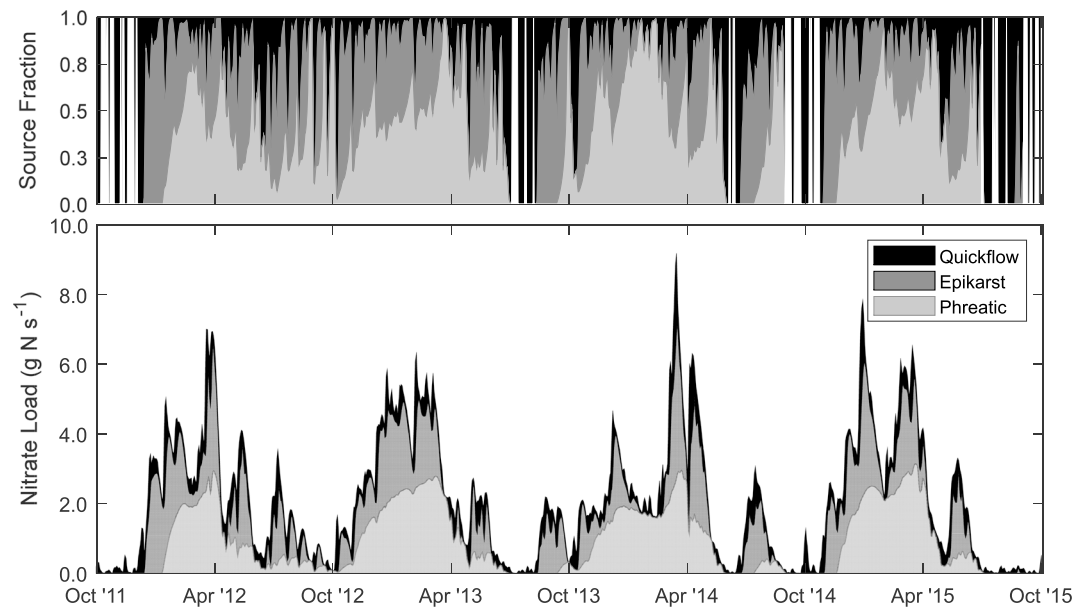


Figure 10. Nitrate source contribution via multiple karst pathways over a two-year period for the optimal model simulation. The top plot shows the fraction of each pathway to the total NO_3^- load. Blank (white) spaces indicate NO_3^- discharge (hence no flux) at the spring. During dry summer periods, particularly when aquifer stores have experienced overpumping, the spring water level will drop below the measurement weir (i.e., no flow). The bottom plot is an area graph and quantifies the NO_3^- load of each pathway as the area between two curves.

pathways are most important for dissolved N fate. This result supports our hypothesis from analysis of the literature based on diluted N concentration data from quick flow (Table 1). The N results of our study extend the past work in Table 1 to show that not only is N concentration of the diffuse flow higher (see Figure 7c) but also these pathways may dominate the annual N load.

3.2.2. Processes Affecting N Exports

Numerical modeling results reflect net removal of N via denitrification within the subterranean karst system (Table 6). There is approximately a 36% removal of N inputs by denitrification in all reservoirs at a rate of $2.2 \text{ mg N} \cdot \text{m}^{-2} \cdot \text{d}^{-1}$. The rate of removal in soil is $1.3 \text{ mg N} \cdot \text{m}^{-2} \cdot \text{d}^{-1}$, and the phreatic and epikarst reservoirs remove approximately 0.2 and $0.7 \text{ mg N} \cdot \text{m}^{-2} \cdot \text{d}^{-1}$, respectively. The relatively low residence time of water in karst aquifers limits the ability of subsurface microbes to further denitrify NO_3^- , and subsequent hydrologic activity promotes the mobilization of accumulated NO_3^- to the springhead. The rates estimated by our model are similar to other karst groundwater systems such as in the Upper Florida (USA) Aquifer where Heffernan et al. (2012) used N isotopic signatures to estimate 32% removal, on average, of N inputs by denitrification. The rates for the 61 springs analyzed in Heffernan et al. (2012) ranged from 0 to $15 \text{ mg N} \cdot \text{m}^{-2} \cdot \text{d}^{-1}$ showcasing the large degree of variability and uncertainty associated with watershed-scale denitrification estimates in karst—even within the same geologic formation. Our results are also consistent with broader groundwater denitrification removal estimates in nonkarst soils ($\sim 5.0 \text{ mg N} \cdot \text{m}^{-2} \cdot \text{d}^{-1}$) and groundwater ($\sim 1.5 \text{ mg N} \cdot \text{m}^{-2} \cdot \text{d}^{-1}$) for the southeastern U.S. region (Seitzinger et al., 2006). These results provide support for the efficacy of relatively simple reservoir models to provide accurate representation of internal aquifer biogeochemical processes.

However, even in the presence of net denitrification we observe an increase in NO_3^- concentration of spring discharge relative to water recharging the aquifer. Modeling results suggest that soil-zone processes, particularly during dryer periods, highly control NO_3^- contamination in the karst watershed (see “soil” in Figure 7c). High rates of evapotranspiration during the dry season remove water, but not N, from the soil column resulting in the relative increase in concentration of N species remaining

Table 5

NO_3^- Budget ($\pm 1\sigma$) for the Royal Spring Basin Showing Inputs (Infiltration and Quick Flow Recharge) and Outputs (Spring, Stream, and Losses Such as Pumping)

Physical NO_3^- Processes			
Inputs	($\text{t N km}^{-2} \text{ yr}^{-1}$)	Outputs	($\text{t N km}^{-2} \text{ yr}^{-1}$)
Infiltration	2.11 (0.30)	Karst spring	1.19 (0.13)
Quick flow	0.12 (0.05)	Surface stream	0.20 (0.06)
		Net aquifer losses	0.46 (0.21)
Total	2.23 (0.31)	Total	1.85 (0.21)

Table 6
Biochemical Reactions ($\pm 1\sigma$) Shown as the Area-Normalized Annual Masses of NO_3^- Denitrified, NH_4^+ Nitrified, and DON Mineralized Within Each Reservoir

Biochemical NO_3^- Processes			
Reservoir	Denitrification ($\text{t N}\cdot\text{km}^{-2}\cdot\text{yr}^{-1}$)	Nitrification ($\text{t N}\cdot\text{km}^{-2}\cdot\text{yr}^{-1}$)	Mineralization ($\text{t N}\cdot\text{km}^{-2}\cdot\text{yr}^{-1}$)
Soil	0.49 (0.28)	0.37 (0.05)	0.27 (0.04)
Epikarst	0.08 (0.06)	0.04 (0.02)	0.03 (0.01)
Phreatic	0.24 (0.15)	0.07 (0.03)	0.05 (0.02)
Total	0.81 (0.39)	0.48 (0.04)	0.35 (0.03)

in the soil. The evapotranspirative concentration of NO_3^- can be quite pronounced in temperate climates, where 60% of precipitation can be removed as evapotranspiration (Hanson, 1991). It is plausible that the highest NO_3^- concentrations observed during the study period (see winter 2012 in Figure 7b) could arise from flushing of highly concentrated soil-N accumulated over the month-long dry period preceding the first large hydrologic event of the wet season. The initial fall/winter flushing event can infiltrate soil and cause highly soluble soil-attached NO_3^- to become entrained within the water and leached via large fractures in the epikarst. Further model support for this idea is observed by comparing relatively dry periods (see “discharge” in Figure 7a) with coinciding periods of higher soil NO_3^- concentration (see soil in Figure 7c). Others have

observed NO_3^- flushing in karst, such as in a chalk (a relatively immature karst) aquifer in Loiret, France (Baran et al., 2008) and a mantled (a karst with a thin surficial sediment deposit) aquifer in Indiana, USA (Wells & Krothe, 1989). Baran et al. (2008) attribute the flushing to NO_3^- accumulation via physical concentration, whereas Wells and Krothe (1989) attribute the flushing to soil water flow through large epikarst fractures. Likewise, in nonkarst systems, evaporation in the vadose zone has been identified—using dual isotopic tracers of NO_3^- ($\delta^{15}\text{N}$ and $\delta^{18}\text{O}$)—as an important mechanism affecting NO_3^- concentration (Huang et al., 2013; Yuan et al., 2012). The authors find relatively little discussion in the literature as to the impact of physical processes leading to concentration and leaching of solutes in karst aquifers. The numerical modeling performed in this study hints to the potential of evapotranspiration to increase observed spring NO_3^- concentrations despite net-denitrifying conditions within the aquifer.

3.2.3. Timing of N Exports From Karst

The timing of N exports from this mature karst basin was compared with the timing of exports from an adjacent immature karst watershed in Ford et al. (2017). While the magnitude of flux from South Elkhorn (2.10 \pm 0.66 $\text{t N}\cdot\text{km}^{-2}\cdot\text{yr}^{-1}$) and Cane Run (1.85 \pm 0.21 $\text{t N}\cdot\text{km}^{-2}\cdot\text{yr}^{-1}$) are comparable, the dynamics controlling the timing of flux vary considerably. At coarse resolution (Figure 11a), the karst-dominated system

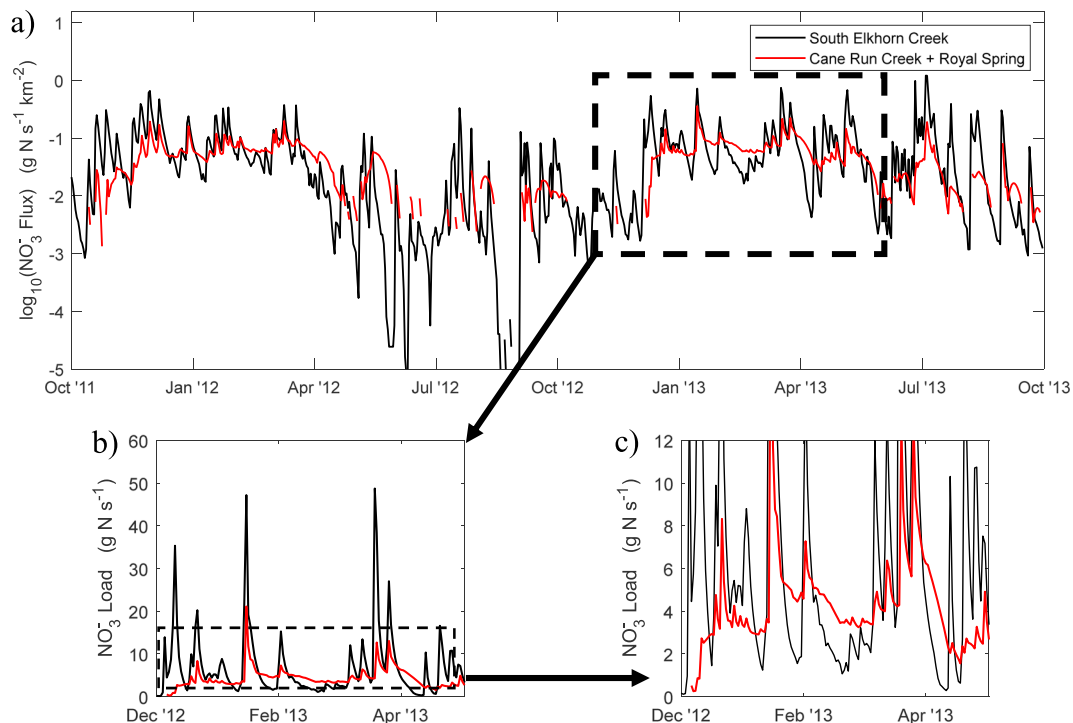


Figure 11. Comparison of cane Run Creek-Royal Spring (CR + RS) to a neighboring immature karst watershed, South Elkhorn Creek (SE) (Ford et al., 2017). (a) Area-normalized NO_3^- load, (b) close-up of six months of NO_3^- load, and (c) highlighting low-flow NO_3^- dynamics in CR + RS.

of this study and fluvial-dominated karst system in Ford et al. (2017) exhibit high similarity in terms of their mean temporal trend. The similarity is reasonable given that the agricultural land surfaces in the two systems apply similar nutrient treatments seasonally and that the two systems experienced the same rainfall distributions. However, closer analyses of the systems (Figure 11b) showed the highly dampened nature of N peaks within the karst watershed even when including both surface and subsurface loading from the karst system. Karst N load peaks were typically on the order of 30% of the nonkarst system response to hydrologic events, and the karst system N load was as low as 15% of the nonkarst system. N loading during hydrologic recession and baseflow periods (see Figure 11c) shows that the karst system consistently produces higher N loads to the downstream water bodies and that it temporally distributes N across active periods more so than the immature karst watershed. Delay of N delivery in karst basins has been discussed in previous work (Croll & Hayes, 1988; Fretwell et al., 2005; Mahler et al., 2008), and the side-by-side comparison presented here extends this discussion. The results occur because of the karst pathway complexity that in turn impacts timing of N loads.

Taken together, the results in Figure 11 highlight the ability of the phreatic karst terrain to act a natural detention basin for NO_3^- that is later received by downstream water bodies. The karst watershed temporally delays the flow of N to downstream waters during hydrologic activity and thereafter exports the N at a more constant rate. Unlike fluvial-dominated systems where over 50% of NO_3^- export may occur during 90th percentile and greater flows (e.g., Royer et al., 2006), modeling results indicate that for our karst-dominated system >90th percentile flows account for less than 25% of NO_3^- export. The sustained downstream delivery of spring water NO_3^- and reduced flow velocities at karst springs (Husic, Fox, Agouridis, et al., 2017; Husic, Fox, Ford, et al., 2017) could prolong the period of bioavailable nutrients to in-stream growth and reduce shearing potential of streams supplied by karst waters. Both of these factors could potentially lead to the development of harmful algal blooms (Franklin et al., 2008; Paerl et al., 2011). Nutrient management scenarios within karst watersheds should not only consider the N concentration of spring discharge but also the timing and length of elevated N concentrations.

4. Conclusions

We have demonstrated the utility of a reservoir model to simulate water and NO_3^- dynamics in an agricultural-karst system. Coupling the reservoir-based model with the four years of N field data provided estimates of the internal epikarst and phreatic processes controlling N fate in agricultural-karst. The numerical modeling approach used herein to estimate water and N fluxes and reduce equifinality has broad applications to other karst modeling studies.

Numerical modeling results also provided insight into the pathways, processes, and timing that control N exports from agricultural-karst systems. Epikarst and phreatic pathways account for nearly 90% of N loading. Further, quick flow pathways dilute downstream NO_3^- contamination. The relative dominance of slow flow in karst is an underdeveloped topic in the water science community. As a second point, evidence is provided that physical processes have a stronger control on N fate in agricultural-karst than biogeochemical processes. N turnover in karst is similar to nonkarst systems, but the dominance of physical processes particularly evapotranspiration leads to net increases in NO_3^- concentration in spring water. As a final note, the timing of N exports from the karst-dominated system suggests that it behaves as a natural detention basin relative to its fluvial-dominated counterpart. To this end, the karst system temporally delays the flow of NO_3^- to downstream waters during storm events and thereafter exports NO_3^- at a more gradual rate distributed over the flood recession. This work highlights the capability of relatively parsimonious modeling to provide meaningful insights into flow and nutrient dynamics of highly complex systems such as karst watersheds.

References

- Albertin, A. R., Sickman, J. O., Pinowska, A., & Stevenson, R. J. (2012). Identification of nitrogen sources and transformations within karst springs using isotope tracers of nitrogen. *Biogeochemistry*, *108*, 219–232. <https://doi.org/10.1007/s10533-011-9592-0>
- Aquilina, L., Ladouche, B., & Dörfli, N. (2006). Water storage and transfer in the epikarst of karstic systems during high flow periods. *Journal of Hydrology*, *327*, 472–485. <https://doi.org/10.1016/j.jhydrol.2005.11.054>
- Baran, N., Lepiller, M., & Mouvet, C. (2008). Agricultural diffuse pollution in a chalk aquifer (Trois Fontaines, France): Influence of pesticide properties and hydrodynamic constraints. *Journal of Hydrology*, *358*, 56–69. <https://doi.org/10.1016/j.jhydrol.2008.05.031>

Acknowledgments

The authors would like to thank the Associate Editor and three anonymous reviewers whose comments helped the authors to greatly improve the quality of this manuscript. The authors would like to acknowledge primary funding from the Kentucky Senate Bill 271B Water Quality program. Steve Workman and Charles Taylor are greatly acknowledged for their contributions and support. The researchers and staff at the Kentucky Geological Survey and the extensive field and laboratory work they performed in the Cane Run Watershed were instrumental in the completion of this work. The authors thank University of Kentucky Research Computing for making available the high-performance computing resources used to perform uncertainty analysis in this study. Lastly, we gratefully acknowledge financial support of this research under National Science Foundation award 1632888, which provided partial support for three of the authors. Calibration data, computer code, and model results will be stored and publicly available at the following <https://figshare.com/s/71d99b86998ff2c9144c>. We have no conflict of interests to report.

- Beven, K. (2006). A manifesto for the equifinality thesis. *Journal of Hydrology*, 320, 18–36. <https://doi.org/10.1016/j.jhydrol.2005.07.007>
- Birgand, F., Skaggs, R. W., Chescheir, G. M., & Gilliam, J. W. (2007). Nitrogen removal in streams of agricultural catchments—A literature review. *Critical Reviews in Environmental Science and Technology*, 37, 381–487. <https://doi.org/10.1080/10643380600966426>
- Bottrel, S. H., & Atkinson, T. C. (1992). Tracer study of flow and storage in the unsaturated zone of a karstic limestone aquifer. In H. Hotzl, & A. Werner (Eds.), *Tracer Hydrology*, (pp. 207–211). Rotterdam: Balkema.
- Bowie, G. L., Mills, W. B., Porcella, D. B., Campbell, C. L., Pagenkopf, J. R., Rupp, G. L., et al. (1985) Rates, constants, and kinetics formulations in surface water quality modeling. U.S. Environmental Protection Agency, Environmental Research Laboratory, Athens, Georgia. EPA/600/3-85/040.
- Boyer, D. G., & Alloush, G. A. (2001). Spatial distribution of nitrogen on grazed karst landscapes. *ScientificWorldJournal*, 1, 809–813. <https://doi.org/10.1100/tsw.2001.374>
- Boyer, D. G., & Pasquarell, G. C. (1995). Nitrate concentrations in karst springs in an extensively grazed area. *Journal of the American Water Resources Association*, 31, 729–736. <https://doi.org/10.1111/j.1752-1688.1995.tb03397.x>
- Buda, A. R., & DeWalle, D. R. (2009). Dynamics of stream nitrate sources and flow pathways during stormflows on urban, forest and agricultural watersheds in central Pennsylvania, USA. *Hydrological Processes*, 23, 3292–3305. <https://doi.org/10.1002/hyp.7423>
- Carvalho, N., Reichstein, M., Ciais, P., Collatz, G. J., Mahecha, M. D., Montagnani, L., et al. (2010). Identification of vegetation and soil carbon pools out of equilibrium in a process model via eddy covariance and biometric constraints. *Global Change Biology*, 16(10), 2813–2829. <https://doi.org/10.1111/j.1365-2486.2010.02173.x>
- Chang, Y., Wu, J., Jiang, G., & Kang, Z. (2017). Identification of the dominant hydrological process and appropriate model structure of a karst catchment through stepwise simplification of a complex conceptual model. *Journal of Hydrology*, 548, 75–87. <https://doi.org/10.1016/J.JHYDROL.2017.02.050>
- Cohen MJ, Lamsal S, Kohnak L V. (2007) Sources, transport and transformations of nitrate-N in the Florida environment special publication SJ2007-SP10. St. Johns River Water Management District. Gainesville, Florida
- Croll, B. T., & Hayes, C. R. (1988). Nitrate and water supplies in the United Kingdom. *Environmental Pollution*, 50, 163–187. [https://doi.org/10.1016/0269-7491\(88\)90190-X](https://doi.org/10.1016/0269-7491(88)90190-X)
- Daly, D., Dassargues, A., Drew, D., Dunne, S., Goldscheider, N., Neale, S., et al. (2002). Main concepts of the “European approach” to karst-groundwater-vulnerability assessment and mapping. *Hydrogeology Journal*, 10, 340–345. <https://doi.org/10.1007/s10040-001-0185-1>
- Davis, J. V., Petersen, J. C., Adamski, J. C., & Freiwald, D. A. (1995). Water-quality assessment of the Ozark Plateaus study unit, Arkansas, Kansas, Missouri, and Oklahoma—Analysis of information on nutrients, suspended sediment, and suspended solids, 1970–92. U.S. Geological Survey; Earth Science Information Center. (No. 95–4042)
- Di, H. J., & Cameron, K. C. (2002). Nitrate leaching in temperate agroecosystems: Sources, factors and mitigating strategies. *Nutrient Cycling in Agroecosystems*, 64(3), 237–256. <https://doi.org/10.1023/A:1021471531188>
- Ekmecki, M. (2005). Pesticide and nutrient contamination in the Kestel polje-Kirkgoz karst springs, southern Turkey. *Environmental Geology*, 49, 19–29. <https://doi.org/10.1007/s00254-005-0022-2>
- Fenton, O., Mellander, P. E., Daly, K., Wall, D. P., Jahangir, M. M. R., Jordan, P., et al. (2017). Integrated assessment of agricultural nutrient pressures and legacies in karst landscapes. *Agriculture, Ecosystems and Environment*, 239, 246–256. <https://doi.org/10.1016/j.agee.2017.01.014>
- Fleury, P., Plagnes, V., & Bakalowicz, M. (2007). Modelling of the functioning of karst aquifers with a reservoir model: Application to Fontaine de Vaucluse (south of France). *Journal of Hydrology*, 345, 38–49. <https://doi.org/10.1016/J.JHYDROL.2007.07.014>
- Ford, W. I., & Fox, J. F. (2015). Isotope-based fluvial organic carbon (ISOFLOC) model: Model formulation, sensitivity, and evaluation. *Water Resources Research*, 51, 4046–4064. <https://doi.org/10.1002/2015WR016999>
- Ford, W. I., Fox, J. F., & Pollock, E. (2017). Reducing equifinality using isotopes in a process-based stream nitrogen model highlights the flux of algal nitrogen from agricultural streams. *Water Resources Research*, 53, 6539–6561. <https://doi.org/10.1002/2017WR020607>
- Fournier, M., Massei, N., Bakalowicz, M., Dussart-Baptista, L., Rodet, J., & Dupont, J. P. (2007). Using turbidity dynamics and geochemical variability as a tool for understanding the behavior and vulnerability of a karst aquifer. *Hydrogeology Journal*, 15, 689–704. <https://doi.org/10.1007/s10040-006-0116-2>
- Franklin, P., Dunbar, M., & Whitehead, P. (2008). Flow controls on lowland river macrophytes: A review. *Science of the Total Environment*, 400, 369–378. <https://doi.org/10.1016/j.scitotenv.2008.06.018>
- Fretwell, B. A., Burgess, W. G., Barker, J. A., & Jefferies, N. L. (2005). Redistribution of contaminants by a fluctuating water table in a microporous, double-porosity aquifer: Field observations and model simulations. *Journal of Contaminant Hydrology*, 78, 27–52. <https://doi.org/10.1016/j.jconhyd.2005.02.004>
- Ghasemizadeh, R., Hellweger, F., Butscher, C., Padilla, I., Vesper, D., Field, M. S., & Alshawabkeh, A. (2012). Review: Groundwater flow and transport modeling of karst aquifers, with particular reference to the North Coast Limestone aquifer system of Puerto Rico. *Hydrogeology Journal*, 20, 1441–1461. <https://doi.org/10.1007/s10040-012-0897-4>
- Goovaerts, P. (2000). Geostatistical approaches for incorporating elevation into the spatial interpolation of rainfall. *Journal of Hydrology*, 228, 113–129. [https://doi.org/10.1016/S0022-1694\(00\)00144-X](https://doi.org/10.1016/S0022-1694(00)00144-X)
- Han, D., Cao, G., McCallum, J., & Song, X. (2015). Residence times of groundwater and nitrate transport in coastal aquifer systems: Daweijia area, northeastern China. *Science of the Total Environment*, 538, 539–554. <https://doi.org/10.1016/j.scitotenv.2015.08.036>
- Hanson, R. L. (1991). Evapotranspiration and droughts. In R. W. Paulson, E. B. Chase, R. S. Roberts, & D. W. Moody (Eds.), *National Water Summary 1988–89—Hydrologic Events and Floods and Droughts*, U.S. Geological Survey Water-Supply Paper (Vol. 2375, pp. 99–104). Reston, VA: United States Geological Survey.
- Hartmann, A. (2017). Experiences in calibrating and evaluating lumped karst hydrological models. In M. Parise, F. Gabrovšek, G. Kaufmann, & N. Ravbar (Eds.), *Advances in Karst Research: Theory, Fieldwork and Applications*. Geological Society, London (pp. 331–340). London: Special Publications.
- Hartmann, A., Antonio Barberá, J., & Andreo, B. (2017). On the value of water quality data and informative flow states in karst modelling. *Hydrology and Earth System Sciences*, 21(12), 5971–5985. <https://doi.org/10.5194/hess-21-5971-2017>
- Hartmann, A., Barberá, J. A., Lange, J., Andreo, B., & Weiler, M. (2013). Progress in the hydrologic simulation of time variant recharge areas of karst systems—Exemplified at a karst spring in southern Spain. *Advances in Water Resources*, 54, 149–160. <https://doi.org/10.1016/j.advwatres.2013.01.010>
- Hartmann, A., Goldscheider, N., Wagoner, T., Lange, J., & Weiler, M. (2014). Karst water resources in a changing world: Approaches, of hydrological modeling. *Reviews of Geophysics*, 52, 218–242. <https://doi.org/10.1002/2013RG000443>

- Hartmann, A., Kobler, J., Kralik, M., Dirnböck, T., Humer, F., & Weiler, M. (2016). Model-aided quantification of dissolved carbon and nitrogen release after windthrow disturbance in an Austrian karst system. *Biogeosciences*, *13*, 159–174. <https://doi.org/10.5194/bg-13-159-2016>
- He, Q., Yang, P., Yuan, W., Jiang, Y., Pu, J., Yuan, D., & Kuang, Y. (2010). The use of nitrate, bacteria and fluorescent tracers to characterize groundwater recharge and contamination in a karst catchment, Chongqing, China. *Hydrogeology Journal*, *18*, 1281–1289. <https://doi.org/10.1007/s10040-010-0594-0>
- Heffernan, J. B., Albertin, A. R., Fork, M. L., Katz, B. G., & Cohen, M. J. (2012). Denitrification and inference of nitrogen sources in the karstic Floridan aquifer. *Biogeosciences*, *9*, 1671–1690. <https://doi.org/10.5194/bg-9-1671-2012>
- Henson, W. R., Huang, L., Graham, W. D., & Ogram, A. (2017). Nitrate reduction mechanisms and rates in an unconfined eogenetic karst aquifer in two sites with different redox potential. *Journal of Geophysical Research: Biogeosciences*, *122*, 1062–1077. <https://doi.org/10.1002/2016JG003463>
- Hirsch, R. M. (2014). Large biases in regression-based constituent flux estimates: Causes and diagnostic tools. *Journal of the American Water Resources Association*, *50*, 1401–1424. <https://doi.org/10.1111/jawr.12195>
- Huang, T., Pang, Z., & Yuan, L. (2013). Nitrate in groundwater and the unsaturated zone in (semi)arid northern China: Baseline and factors controlling its transport and fate. *Environment and Earth Science*, *70*, 145–156. <https://doi.org/10.1007/s12665-012-2111-3>
- Husic, A. (2015). Sediment organic carbon fate and transport in a fluviokarst. Master's Thesis, University of Kentucky, Lexington, Kentucky
- Husic, A., Fox, J., Adams, E., Backus, J., Pollock, E., Ford, W., & Agouridis, C. (2019). Inland impacts of atmospheric river and tropical cyclone extremes on nitrate transport and stable isotope measurements. *Environment and Earth Science*, *78*, 36. <https://doi.org/10.1007/s12665-018-8018-x>
- Husic, A., Fox, J. F., Agouridis, C., Currens, J. C., Ford, W. I., & Taylor, C. J. (2017). Sediment carbon fate in phreatic karst (Part 1): Conceptual model development. *Journal of Hydrology*, *549*, 179–193. <https://doi.org/10.1016/j.jhydrol.2017.03.052>
- Husic, A., Fox, J. F., Ford, W. I., Agouridis, C., Currens, J. C., & Taylor, C. J. (2017). Sediment carbon fate in phreatic karst (Part 2): Numerical model development and application. *Journal of Hydrology*, *549*, 208–219. <https://doi.org/10.1016/J.JHYDROL.2017.03.059>
- Jones, A. L., & Smart, P. L. (2005). Spatial and temporal changes in the structure of groundwater nitrate concentration time series (1935–1999) as demonstrated by autoregressive modelling. *Journal of Hydrology*, *310*, 201–215. <https://doi.org/10.1016/j.jhydrol.2005.01.002>
- Katz, B. G., Chelette, A. R., & Pratt, T. R. (2004). Use of chemical and isotopic tracers to assess nitrate contamination and ground-water age, Woodville Karst Plain, USA. *Journal of Hydrology*, *289*, 36–61. <https://doi.org/10.1016/j.jhydrol.2003.11.001>
- Katz, B. G., Griffin, D. W., McMahon, P. B., Harden, H. S., Wade, E., Hicks, R. W., & Chanton, J. P. (2010). Fate of effluent-borne contaminants beneath septic tank drainfields overlying a karst aquifer. *Journal of Environmental Quality*, *39*, 1181. <https://doi.org/10.2134/jeq2009.0244>
- KGS (Kentucky Geological Survey) (2018). Groundwater information via the Kentucky Groundwater Data Repository. In: Kentucky Geol. Surv. <https://kgs.uky.edu/kgsweb/DataSearching/watersearch.asp>
- Knierim, K. J., Pollock, E., & Hays, P. D. (2013). Using isotopes of dissolved inorganic carbon species and water to separate sources of recharge in a Cave Spring, northwestern Arkansas, USA. *Acta Carsologica*, *42*, 261–276.
- Kovačić, G. (2010). Hydrogeological study of the Malenscica karst spring (SW Slovenia) by means of a time series analysis. *Acta Carsologica*, *39*, 201–215.
- KWW (Kentucky Water Watch) (2016). Volunteers protecting Kentucky waterways. In: Kentucky Water Watch. <https://water.ky.gov/www/Pages/default.aspx>
- Liu, C.-Q., Li, S.-L., Lang, Y.-C., & Xiao, H.-Y. (2006). Using $\delta^{15}\text{N}$ and $\delta^{18}\text{O}$ values to identify nitrate sources in karst groundwater, Guiyang, southwest China. *Environmental Science & Technology*, *40*, 6925–6933. <https://doi.org/10.1021/es0610129>
- Liu, D., Guo, S., Wang, Z., Liu, P., Yu, X., Zhai, Q., & Zou, H. (2018). Statistics for sample splitting for the calibration and validation of hydrological models. *Stochastic Environmental Research and Risk Assessment*, *32*(11), 3099–3116. <https://doi.org/10.1007/s00477-018-1539-8>
- Long, A. J. (2009). Hydrograph separation for karst watersheds using a two-domain rainfall-discharge model. *Journal of Hydrology*, *364*, 249–256. <https://doi.org/10.1016/j.jhydrol.2008.11.001>
- Long, A. J., Sawyer, J. F., & Putnam, L. D. (2008). Environmental tracers as indicators of karst conduits in groundwater in South Dakota, USA. *Hydrogeology Journal*, *16*, 263–280. <https://doi.org/10.1007/s10040-007-0232-7>
- Mahler, B. J., & Garner, B. D. (2009). Using nitrate to quantify quick flow in a karst aquifer. *Ground Water*, *47*, 350–360. <https://doi.org/10.1111/j.1745-6584.2008.00499.x>
- Mahler, B. J., Valdes, D., Musgrove, M., & Massei, N. (2008). Nutrient dynamics as indicators of karst processes: Comparison of the Chalk aquifer (Normandy, France) and the Edwards aquifer (Texas, U.S.A.). *Journal of Contaminant Hydrology*, *98*, 36–49. <https://doi.org/10.1016/j.jconhyd.2008.02.006>
- Mahoney, D. T., Al Aamery, N., Fox, J. F., Riddle, B., Ford, W., Wang, Y. T., & Fox, J. F. (2018). Equilibrium sediment exchange in the Earth's critical zone: Evidence from sediment fingerprinting with stable isotopes and watershed modeling. *Journal of Soils and Sediments*, 1–25. <https://doi.org/10.1007/s11368-018-2208-8>
- Mahoney, D. T., Fox, J. F., & Al Aamery, N. (2018). Watershed erosion modeling using the probability of sediment connectivity in a gently rolling system. *Journal of Hydrology*, *561*, 862–883. <https://doi.org/10.1016/j.jhydrol.2018.04.034>
- Malik, P., & Vojtková, S. (2012). Use of recession-curve analysis for estimation of karstification degree and its application in assessing overflow/underflow conditions in closely spaced karstic springs. *Environment and Earth Science*, *65*, 2245–2257. <https://doi.org/10.1007/s12665-012-1596-0>
- Mangin, A. (1984). The use of autocorrelation and spectral analyses to obtain a better understanding of hydrological systems. *Journal of Hydrology*, *67*(1–4), 25–43. [https://doi.org/10.1016/0022-1694\(84\)90230-0](https://doi.org/10.1016/0022-1694(84)90230-0)
- Markovic, T., Miko, S., Kapelj, S., Buljan, R., Larva, O., & Peh, Z. (2006). Behaviour of metals and nutrients in soils and groundwater of a karst Polje. *Journal of Geochemical Exploration*, *88*, 124–129. <https://doi.org/10.1016/j.gexplo.2005.08.024>
- Mazzilli, N., Guinot, V., & Jourde, H. (2012). Sensitivity analysis of conceptual model calibration to initialisation bias. Application to karst spring discharge models. *Advances in Water Resources*, *42*, 1–16. <https://doi.org/10.1016/j.advwatres.2012.03.020>
- Mellander, P.-E., Melland, A. R., Jordan, P., Wall, D. P., Murphy, P. N. C., & Shortle, G. (2012). Quantifying nutrient transfer pathways in agricultural catchments using high temporal resolution data. *Environmental Science & Policy*, *24*, 44–57.
- Miller, M. P., Tesoriero, A. J., Hood, K., Terziotti, S., & Wolock, D. M. (2017). Estimating discharge and nonpoint source nitrate loading to streams from three end-member pathways using high-frequency water quality data. *Water Resources Research*, *53*, 10,201–10,216. <https://doi.org/10.1002/2017WR021654>

- Moers, H. D., & Alexander, E. C. (1994). Contribution of spray irrigation of wastewater to groundwater contamination in the karst of southeastern Minnesota, USA. *Applied Hydrogeology*, 2(1), 34–44. <https://doi.org/10.1007/s100400050041>
- Moriasi, D. N., Arnold, J. G., van Liew, M. W., Bingner, R. L., Harmel, R. D., & Veith, T. L. (2007). Model evaluation guidelines for systematic quantification of accuracy in watershed simulations. *Transactions of the American Society of Agricultural and Biological Engineers*, 50, 885–900.
- Moriasi, D. N., Wilson, B. N., Douglas-Mankin, K. R., Arnold, J. G., & Gowda, P. H. (2012). Hydrologic and water quality models: Use, calibration, and validation. *Transactions of the American Society of Agricultural and Biological Engineers*, 55(4), 1241–1247. <https://doi.org/10.13031/2013.42265>
- Mudarra, M., Andreo, B., Barberá, J. A., & Mudry, J. (2014). Hydrochemical dynamics of TOC and NO₃⁻ contents as natural tracers of infiltration in karst aquifers. *Environment and Earth Science*, 71, 507–523. <https://doi.org/10.1007/s12665-013-2593-7>
- Mulholland, P. J., Helton, A. M., Poole, G. C., Hall, R. O., Hamilton, S. K., Peterson, B. J., et al. (2008). Stream denitrification across biomes and its response to anthropogenic nitrate loading. *Nature*, 452, 202–205. <https://doi.org/10.1038/nature06686>
- Musgrove, M., Opsahl, S. P., Mahler, B. J., Herrington, C., Sample, T. L., & Banta, J. R. (2016). Source, variability, and transformation of nitrate in a regional karst aquifer: Edwards aquifer, central Texas. *Science of the Total Environment*, 568, 457–469. <https://doi.org/10.1016/j.scitotenv.2016.05.201>
- Nikolaidis, N. P., Bouraoui, F., & Bidoglio, G. (2013). Hydrologic and geochemical modeling of a karstic Mediterranean watershed. *Journal of Hydrology*, 477, 129–138. <https://doi.org/10.1016/j.jhydrol.2012.11.018>
- Obeidat, M. M., Ahmad, F. Y., Hamouri, N. A., Massadeh, A. M., & Athamneh, F. S. (2008). Assessment of nitrate contamination of karst springs, Bani Kanana, northern Jordan. *Revista Mexicana de Ciencias Geológicas*, 25, 426–437.
- Opsahl, S. P., Musgrove, M., & Slattery, R. N. (2017). New insights into nitrate dynamics in a karst groundwater system gained from in situ high-frequency optical sensor measurements. *Journal of Hydrology*, 546, 179–188. <https://doi.org/10.1016/j.jhydrol.2016.12.038>
- Paerl, H. W., Hall, N. S., & Calandrino, E. S. (2011). Controlling harmful cyanobacterial blooms in a world experiencing anthropogenic and climatic-induced change. *Science of the Total Environment*, 409, 1739–1745. <https://doi.org/10.1016/j.scitotenv.2011.02.001>
- Palanisamy, B., & Workman, S. R. (2014). Hydrologic modeling of flow through sinkholes located in streambeds of Cane Run Stream, Kentucky. *Journal of Hydrologic Engineering*, 20(5), 04014066. [https://doi.org/10.1061/\(ASCE\)HE.1943-5584.0001060](https://doi.org/10.1061/(ASCE)HE.1943-5584.0001060)
- Panno, S. V., Hackley, K. C., Hwang, H. H., & Kelly, W. R. (2001). Determination of the sources of nitrate contamination in karst springs using isotopic and chemical indicators. *Chemical Geology*, 179, 113–128. [https://doi.org/10.1016/S0009-2541\(01\)00318-7](https://doi.org/10.1016/S0009-2541(01)00318-7)
- Paylor, R., & Currens, J. C. (2004). Royal Springs karst groundwater travel time investigation. A report prepared for Georgetown Municipal Water and Sewer Service. Lexington, KY
- Peterson, E. W., Davis, R. K., Brahana, J. V., & Orndorff, H. A. (2002). Movement of nitrate through regolith covered karst terrane, northwest Arkansas. *Journal of Hydrology*, 256, 35–47. [https://doi.org/10.1016/S0022-1694\(01\)00525-X](https://doi.org/10.1016/S0022-1694(01)00525-X)
- Phillips, J. D., Martin, L. L., Nordberg, V. G., & Andrews, W. A. (2004). Divergent evolution in fluvio-karst landscapes of central Kentucky. *Earth Surface Processes and Landforms*, 29, 799–819. <https://doi.org/10.1002/esp.1070>
- Pronk, M., Goldscheider, N., Zopfi, J., & Zwahlen, F. (2009). Percolation and particle transport in the unsaturated zone of a karst aquifer. *Ground Water*, 47, 361–369. <https://doi.org/10.1111/j.1745-6584.2008.00509.x>
- Reichstein, M., Bednorz, F., Broll, G., & Kätterer, T. (2000). Temperature dependence of carbon mineralisation: Conclusions from a long-term incubation of subalpine soil samples. *Soil Biology and Biochemistry*, 32, 947–958. [https://doi.org/10.1016/S0038-0717\(00\)00002-X](https://doi.org/10.1016/S0038-0717(00)00002-X)
- Rowden, R. D., Libra, R. D., & Liu, H. (1998). Shallow groundwater and surface water monitoring of the Silver Creek sub-basin within the Big Spring Basin 1986–1995: A summary review. Des Moines, IA
- Rowden, R. D., Liu, H., & Libra, R. D. (2001). Results from the Big Spring basin water quality monitoring and demonstration projects, Iowa, USA. *Hydrogeology Journal*, 9, 487–497. <https://doi.org/10.1007/s100400100150>
- Royer, T. V., David, M. B., & Gentry, L. E. (2006). Timing of riverine export of nitrate and phosphorus from agricultural watersheds in Illinois: Implications for reducing nutrient loading to the Mississippi River. *Environmental Science & Technology*, 40, 4126–4131. <https://doi.org/10.1021/es052573n>
- Sarrazin, F., Hartmann, A., Pianosi, F., & Wagener, T. (2018). V2Karst V1.1: A parsimonious large-scale integrated vegetation–recharge model to simulate the impact of climate and land cover change in karst regions. *Geoscientific Model Development*, 11, 4933–4964.
- Schilling, K. E., & Helmers, M. (2008). Tile drainage as karst: Conduit flow and diffuse flow in a tile-drained watershed. *Journal of Hydrology*, 349, 291–301. <https://doi.org/10.1016/j.jhydrol.2007.11.014>
- Seitzinger, S., Harrison, J., Bohlke, J., Bouwman, A., Lowrance, R., Peterson, B., et al. (2006). Denitrification across landscapes and waterscapes: A synthesis. *Ecological Applications*, 16(6), 2064–2090. [https://doi.org/10.1890/1051-0761\(2006\)016\[2064:DALAWA\]2.0.CO;2](https://doi.org/10.1890/1051-0761(2006)016[2064:DALAWA]2.0.CO;2)
- Silvestro, F., Gabellani, S., Rudari, R., Delogu, F., Laioli, P., & Boni, G. (2015). Uncertainty reduction and parameter estimation of a distributed hydrological model with ground and remote-sensing data. *Hydrology and Earth System Sciences*, 19, 1727–1751. <https://doi.org/10.5194/hess-19-1727-2015>
- Sinha, E., & Michalak, A. M. (2016). Precipitation dominates interannual variability of riverine nitrogen loading across the continental United States. *Environmental Science & Technology*, 50, 12,874–12,884. <https://doi.org/10.1021/acs.est.6b04455>
- Spangler, L. E. (1982). Karst hydrogeology of northern Fayette and southern Scott counties, Kentucky. Master's Thesis, University of Kentucky, Lexington, Kentucky
- Stueber, A. M., & Criss, R. E. (2005). Origin and transport of dissolved chemicals in a karst watershed, southwestern Illinois. *Journal of the American Water Resources Association*, 41, 267–290. <https://doi.org/10.1111/j.1752-1688.2005.tb03734.x>
- Swanson, E. (2004). Analysis of phosphorus in Spring Creek and Sheridan Lake in the Black Hills of South Dakota. Doctoral Dissertation, South Dakota School of Mines and Technology, Rapid City, South Dakota
- Taylor, C. J. (1992). Ground-water occurrence and movement associated with sinkhole alignments in the Inner Bluegrass Karst Region of central Kentucky. Master's Thesis, University of Kentucky, Lexington, Kentucky.
- Tesoriero, A. J., Duff, J. H., Saad, D. A., Spahr, N. E., & Wolock, D. M. (2013). Vulnerability of streams to legacy nitrate sources. *Environmental Science & Technology*, 47, 3623–3629. <https://doi.org/10.1021/es305026x>
- Tesoriero, A. J., & Puckett, L. J. (2011). O₂ reduction and denitrification rates in shallow aquifers. *Water Resources Research*, 47, W12522. <https://doi.org/10.1029/2011WR010471>
- Thraillkill, J., Sullivan, S. B., & Gouzie, D. R. (1991). Flow parameters in a shallow conduit-flow carbonate aquifer, Inner Bluegrass Karst Region, Kentucky, USA. *Journal of Hydrology*, 129, 87–108. [https://doi.org/10.1016/0022-1694\(91\)90046-K](https://doi.org/10.1016/0022-1694(91)90046-K)
- Toran, L., & White, W. B. (2005). Variation in nitrate and calcium as indicators of recharge pathways in Nolte Spring, PA. *Environmental Geology*, 48, 854–860. <https://doi.org/10.1007/s00254-005-0018-y>

- Tritz, S., Guinot, V., & Jourde, H. (2011). Modelling the behaviour of a karst system catchment using non-linear hysteretic conceptual model. *Journal of Hydrology*, 397, 250–262. <https://doi.org/10.1016/j.jhydrol.2010.12.001>
- Tzoraki, O., & Nikolaidis, N. P. (2007). A generalized framework for modeling the hydrologic and biogeochemical response of a Mediterranean temporary river basin. *Journal of Hydrology*, 346, 112–121. <https://doi.org/10.1016/j.jhydrol.2007.08.025>
- UKAg (University of Kentucky Agriculture Weather Center) (2007). Research farm climate data. https://www.wagwx.ca.uky.edu/ky/data.php#Spindletop_Farm_Data. Accessed 6 Jan 2018
- UKCAFE (University of Kentucky College of Agriculture Food and the Environment) (2011). Cane Run and Royal Spring watershed-based plan, version 5. EPA Project Number C9994861-06. In: Univ. Kentucky Coll. Agric. Food Environ. www.bae.uky.edu/CaneRun/PDFs/Cane_Run_WBP_2011.pdf. Accessed 6 Jan 2018
- Wellen, C., Kamran-Disfani, A.-R., & Arhonditsis, G. B. (2015). Evaluation of the current state of distributed watershed nutrient water quality modeling. *Environmental Science & Technology*, 49, 3278–3290. <https://doi.org/10.1021/es5049557>
- Wells, E. R., & Krothe, N. C. (1989). Seasonal fluctuation in $\delta^{15}\text{N}$ of groundwater nitrate in a mantled karst aquifer due to macropore transport of fertilizer-derived nitrate. *Journal of Hydrology*, 112, 191–201. [https://doi.org/10.1016/0022-1694\(89\)90188-1](https://doi.org/10.1016/0022-1694(89)90188-1)
- White, W. B. (2002). Karst hydrology: Recent developments and open questions. *Engineering Geology*, 65, 85–105. [https://doi.org/10.1016/S0013-7952\(01\)00116-8](https://doi.org/10.1016/S0013-7952(01)00116-8)
- Williams, P. W. (2008). The role of the epikarst in karst and cave hydrogeology: A review. *International Journal of Speleology*, 74(1), 254–210. <https://doi.org/10.2307/2423146>
- Yuan, L., Pang, Z., & Huang, T. (2012). Integrated assessment on groundwater nitrate by unsaturated zone probing and aquifer sampling with environmental tracers. *Environmental Pollution*, 171, 226–233. <https://doi.org/10.1016/j.envpol.2012.07.027>
- Yuan, Y., Bingner, R. L., & Rebich, R. A. (2001). Evaluation of AnnAGNPS on Mississippi Delta MSEA watersheds. *Transactions of ASAE*, 44(5), 1183–1190. <https://doi.org/10.13031/2013.6448>
- Yue, F. J., Li, S. L., Liu, C. Q., Lang, Y. C., & Ding, H. (2015). Sources and transport of nitrate constrained by the isotopic technique in a karst catchment: An example from southwest China. *Hydrological Processes*, 29, 1883–1893. <https://doi.org/10.1002/hyp.10302>
- Zhu, J., Currens, J. C., & Dinger, J. S. (2011). Challenges of using electrical resistivity method to locate karst conduits—A field case in the Inner Bluegrass Region, Kentucky. *Journal of Applied Geophysics*, 75, 523–530. <https://doi.org/10.1016/j.jappgeo.2011.08.009>